THE ROLE OF LIPID PHOSPHATE PHOSPHATASE 3 IN CARDIAC ENERGY METABOLISM

by

Anu Jose

Submitted in partial fulfilment of the requirements
for the degree of Master of Science

at

Dalhousie University
Halifax, Nova Scotia
June 2023

Dalhousie University is located in Mi'kma'ki, the
ancestral and unceded territory of the Mi'kmaq.
We are all Treaty people.

Table of Contents

List of tables

List of figures

Abstract

Lysophosphatidic acid (LPA) is a bioactive lipid that is generated by autotaxin (ATX) in circulation and is implicated in obesity induced cardiomyopathy. LPA signaling is terminated by lipid phosphate phosphatase 3 (LPP3) through dephosphorylation to monoacylglycerol (MAG). Plasma LPA increases with obesity and contributes to cardiovascular complications. Prior data from our lab show that heterozygous whole body ATX knockout mice are partially protected from diet-induced obesity and cardiomyocyte contractile dysfunction. We hypothesized that reducing LPA signaling in cardiomyocytes by selectively overexpressing LPP3 in the heart protects from obesity-induced cardiomyopathy. In mice with cardiomyocyte-specific LPP3 overexpression ($LPP3^{OE}$) plasma LPA levels were reduced by 57% and 41% in low fat diet fed (LFD) males and females, respectively, compared to the LFD control group, which was associated with enhanced pyruvate-linked mitochondrial respiration in $LPP3^{OE}$ hearts. After 20 weeks of high fat diet (HFD) feeding, female $LPP3^{OE}$ mice showed reduced body weight gain and protection from impaired insulin sensitivity and cardiac dysfunction, which was paralleled by reduced plasma LPA levels and enhanced pyruvate linked mitochondrial respiration in cardiac myofibers compared to HFD-fed control mice. Female $LPP3^{OE}$ mice were also protected from HFD-induced cardiac hypertrophy. Interestingly, this cardiometabolic protective effect was not observed in HFD-fed male $LPP3^{\mathbf{OE}}$ mice. Taken together, my thesis work identified LPP3 in cardiomyocytes as a regulator of circulating LPA levels, mitochondrial metabolism, and cardiac function. This work also suggests that targeting the LPA-LPP3 signaling pathway could be explored as a therapeutic strategy to treat obesity-induced cardiomyopathy, particularly in women.

List of Abbreviations Used

ADP	Adenosine diphosphate
ANOVA	Analysis of variance formula
APV	Aortic peak velocity
ATK KO Het	Heterozygous autotaxin knockout
ATP	Adenosine triphosphate
ATX	Autotaxin
B2M	β_2 microglobulin
BAT	Brown adipose tissue
BCA	Bicinchoninic acid
BMI	Body mass index
BSA	Bovine serum albumin
C1P	Ceramide-1-phosphate
Cacl2	Calcium cholride
CD36	cluster of differentiation 36
cDNA	Complimentary DNA
CDS	Coding sequence
CMLPP3-/-	Cardiomyocyte specific LPP3 knockdown
CO2	Carbon dioxide
CPT	Carnitine palmitoyl-transferase
CPT1	Carnitine palmitoyltransferase 1
CVD	Cardiovascular disease

DAG	Diacylglycerol
DIO	Diet-induced obesity
DMEM	Dulbecco's modified eagle medium
DMEM-HG	Dulbecco's modified eagle medium high glucose
DNA	Deoxyribonucleic acid
DTT	Dithiothreitol
E/A	ratio between early (E) and late (atrial - A) ventricular filling velocity
ECG	Echocardiogram
ECL	Enhanced chemiluminescent
EDTA	Ethylenediamine tetraacetic acid
EGTA	ethylene glycol-bis(β-aminoethyl ether)-N,N,N',N'-tetraacetic acid
ELISA	Enzyme linked immunosorbent assay
ENPP2	Ectonucleotide pyrophosphatase/phosphodiesterase 2
ERK	Extracellular receptor kinase
FA	Fatty acid
FAO	Fatty acid oxidation
FBS	Fetal bovine serum
FCCP	Carbonyl cyanide-p-trifluoromethoxyphenylhydrazone
FFA	Free fatty acid
GAPDH	Glyceraldehyde 3-phosphate dehydrogenase
GLUT	Glucose transport protein
GPCR	G protein-coupled receptor
GSK3	Glycogen synthase kinase 3
GTT	Glucose tolerance test

HCL	Hydrochloric acid
HEPES	2-[4-(2-hydroxyethyl)piperazin-1-yl]ethanesulfonic acid
HFD	High fat diet
HFHS	High fat high sucrose
HPRT1	Hypoxanthine-guanine phosphoribosyltransferase
HRP	Horse radish peroxidase
IR	Insulin receptor
IRS	Insulin receptor substrate
ITT	Insulin tolerance test
IVCT	Isovolumic contraction time
IVRT	Isovolumic relaxation time
kcal	Kilo calories
Kcl	Potassium chloride
KH2PO4	Potassium dihydrogen phosphate
LFD	Low fat diet
LPA	Lysophosphatidic acid
LPC	Lysophosphatidyl choline
LPP1-3	Lipid phosphate phosphatase 1-3
MAG	Monoacylglycerol
MEM	Minimum essential medium
Mgcl2	Magnessium chloride
MPC	Mitochondrial pyruvate carrier
mRNA	Messenger RNA
mTORC	Mammalian target of rapamycin complex

Na2HPO4	Sodium phosphate dibasic dihydrate
Nacl	Sodium chloride
NF-κb	Nuclear factor kappa light chain enhancer of activated B
nM	Nanomolar
OXPHOS	Oxidative phosphorylation
PA	Phosphatidic acid
PAGE	Polyacrylamide gel electrophoresis
pAKT S473	Phospho AKT serine 473
pAKT T308	Phospho AKT Threonine 308
PBS	Phosphate-buffered saline
PC	Palmitoyl carnitine
PCR	Polymerase chain reaction
PDH	Pyruvate dehydrogenase
PDK	Phosphoinositide-dependent kinase
PDK1	3-Phosphoinositide-dependent kinase 1
PGAT	Perigonadal adipose tissue
PI3K	Phosphatidylinositol-3-kinase
PIP3	Phosphatidylinositol-3,4,5-triphosphate
PKB	Protein kinase B
PKC	Protein kinase C
PLD	Phospholipase D
PPAP2B	Phosphatidic acid phosphatase type 2B
Pyr	Pyruvate
qPCR	Quantitative polymerase chain reaction

Rho	Ras homologous
RNA	Ribonucleic acid
ROS	Reactive oxygen species
RPL7	Ribosomal protein L7
RSM	Rodent surgical monitor
S1P	Sphingosine-1-phosphate
P70S6K	Ribosomal protein S6 kinase beta1
SDS	Sodium dodecyl sulphate
SEM	Standard error of the mean
siRNA	Small interfering RNA
T2D	Type 2 diabetes
TAG	Triacylglycerol
TBS	Tris-buffered saline
TBS-T	T tris-buffered saline-tween
TCA	Tricarboxylic acid
TCA	Tricarboxylic cycle
VLDL	Very low density lipoprotein
WT	Wild type

Acknowledgements

I am sincerely grateful to my supervisor Dr. Petra Kienesberger for the guidance, expertise, and continuous support throughout the research process. The invaluable insights and constructive feedback have been instrumental in shaping this thesis. I extend my heartfelt thanks to the members of my thesis committee Dr. Barbara Karten and Dr. Aarnoud Van Der Spoel for their time, expertise, and valuable suggestions. Their input and scholarly advice have greatly enriched the quality of this work. Thank you to the additional faculty members at DMNB, especially Dr. Thomas Pulinilkunnil, who I could always turn to for advice on both scientific and personal matters. I am grateful to my fellow researchers, colleagues, and peers Maggie Pickard, Adithi Pisapati, Esther Yi, Dr. Shanmughasundaram Pakkiriswami, Angella Mercer, Yadab Paudel, Dr. Logan Slade for their stimulating discussions, encouragement, and support throughout this thesis journey. Their intellectual contributions and collaborative spirit have been truly inspiring.

I am deeply thankful to my family especially my husband Reen Babu who has been there for me as an emotional support and friends for their unwavering support, love, and encouragement throughout my academic pursuits. Their belief in my abilities and their patience during challenging times have been the cornerstone of my success. I would like to acknowledge Dalhousie Medicine New Brunswick for providing the necessary resources, facilities, and infrastructure that facilitated the smooth progress of my research. Their commitment to academic excellence has been crucial in shaping my academic journey. I gratefully acknowledge the financial support received from DMNB and DMRF. Their support not only enabled me to undertake this research but also provided me with valuable opportunities for professional development. I extend my appreciation to any other

individuals or organizations who have contributed to my research or provided assistance in any form. Your support has made a significant impact on the successful completion of this thesis. Lastly, I would like to express my deepest gratitude to all those whose names may not appear here but who have contributed in various ways to my academic growth and the completion of this thesis.

CHAPTER 1: INTRODUCTION

1.1 Obesity as a risk factor for cardiovascular diseases

1.1.1 Prevalence and etiology of obesity

According to the World health organization (WHO), obesity is defined as the accumulation of excessive fat that presents a risk to health. In 1997, the WHO declared obesity as a major public health problem and global epidemic. As per obesity atlas 2022 (The World Obesity Federation, www.worldobesity.org), 7 out of 10 adults and almost 8 out of 11 children are at risk for obesity in Canada. Today 39% (39% of men and 40% of women) of adults aged 18 or over are living with overweight and 13% are living with obesity. A sedentary lifestyle and lack of physical activity along with the consumption of energy rich, highly processed food contribute to excess body fat accumulation. It has been shown that overweight and obese individuals have an elevated risk of developing cardiovascular diseases (CVDs)[1]. The global increase in obesity prevalence and the associated elevated risk of CVDs burdens health care systems in many countries. In 2020, approximately 19.1 million deaths were attributed to CVD globally. According to the Heart disease and Stroke Statistics update report from 2017, the total direct medical costs of CVD is estimated to increase from $396 billion to $918 billion between 2012 to 2030[2]. With increasing prevalence of obesity in populations with a longer life span, there is a need to evaluate mechanisms underlying obesity-related cardiac dysfunction and to improve the CVD management of patients with obesity through future research.

1.1.2 Mechanisms underlying cardiovascular diseases in obesity

Obesity is a complex condition that can significantly impact cardiovascular health. Obesity is risk factor for a variety of CVDs including atherosclerosis and coronary artery disease, cardiomyopathy, arrhythmias, myocardial infarction, and heart failure which are the main causes of death. Comorbidities including dyslipidemia, hypertension, diabetes, insulin resistance and systemic inflammation contribute to obesity related CVDs[3].

Adipose tissue is the primary site for storing fats in the form of triacylglycerols (TAGs). During obesity, adipose tissue can become dysfunctional and unable to store excess lipids properly[4]. This can lead to the increased release of free fatty acids (FFAs) into the bloodstream due to abnormally elevated lipolysis. Excess circulating FFAs can be taken up by non-adipose tissues, such as the liver, skeletal muscle, and pancreas, resulting in increased ectopic lipid accumulation[5]. Non-adipose tissues are not adapted for lipid storage and begin to accumulate fatty acids (FAs) and their metabolites giving rise to tissue lipotoxicity, wherein fat metabolites cause cell stress, dysfunction, and death. Lipotoxicity can lead to ER stress, inflammation, and apoptosis, and impair cellular insulin signaling resulting in tissue and whole-body insulin resistance[6]. Also, in situations of lipid overload, excess FFAs can lead to the accumulation of harmful lipid intermediates such as diacylglycerol (DAG) and ceramides[7]. These intermediates can activate various signaling pathways that interfere with cellular functions, leading to insulin resistance and impaired glucose metabolism. Under obese conditions excess glucose is converted to TAGs through *de novo* lipogenesis in the liver. These excess TAGs are packaged into very low density lipoproteins (VLDL) and released into the blood stream[8]. This process also can increase ectopic lipid accumulation through excess lipoprotein uptake and hydrolysis[9]. The

metabolic changes in adipose tissue during obesity not only induce insulin resistance, but also affect cardiac energy metabolism and can lead to cardiomyopathy, which is characterized by changes in metabolism, structure and function of the myocardium that are not directly attributable to confounding factors including coronary artery disease and hypertension[10]. Cardiomyopathy is the weakening of heart muscle which makes it harder for the heart to pump sufficient blood required to sustain bodily functions.

1.2 Cardiac energy metabolism

The heart requires a continuous supply of nutrients to meet its high metabolic demand and for proper functioning. It is estimated that the human myocardium requires 6 kg of ATP per day to maintain uninterrupted contraction[11]. The healthy heart is metabolically flexible and depends mainly on the oxidation of long-chain fatty acids and glucose for ATP production (Figure 1.2), but is also able to use lactate, amino acids, and ketone bodies as energy substrates[12]. This metabolic flexibility helps to maintain contractile function under different physiological and pathophysiological conditions. Randle *et al*. proposed that the utilization of one nutrient (fatty acids) in inhibited by the use of the other (glucose)[13]. Obesity induced insulin resistance and the corresponding surge in circulating lipids impair the metabolic flexibility of the heart by forcing the heart to exceedingly rely on the use of fatty acids for ATP production and reducing the use of glucose (Randle cycle)[13],[14]. Since, fatty acid metabolism produces less ATP per molecule of oxygen consumed than glucose, the obese heart tends to show decreased efficiency compared to the obese heart[15]. This metabolic inflexibility can promote mitochondrial dysfunction, increased ROS production, and apoptosis, which can cause pathological changes in myocardial structure and function leading to cardiomyopathy[16].

A

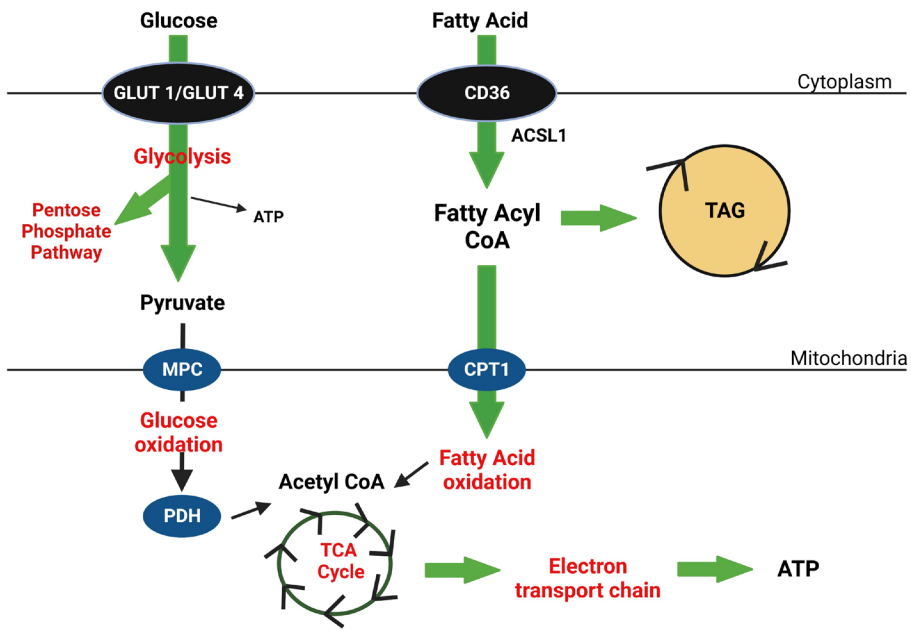

B

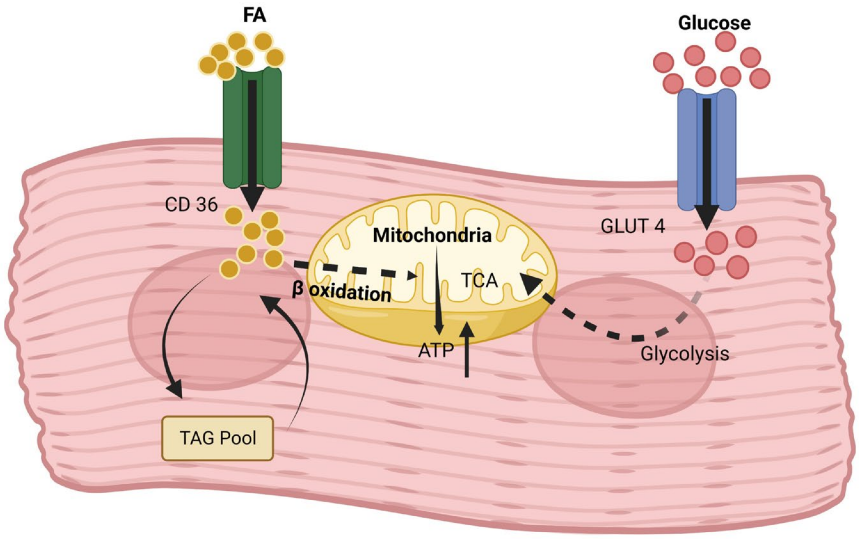

Healthy Cardiomyocyte

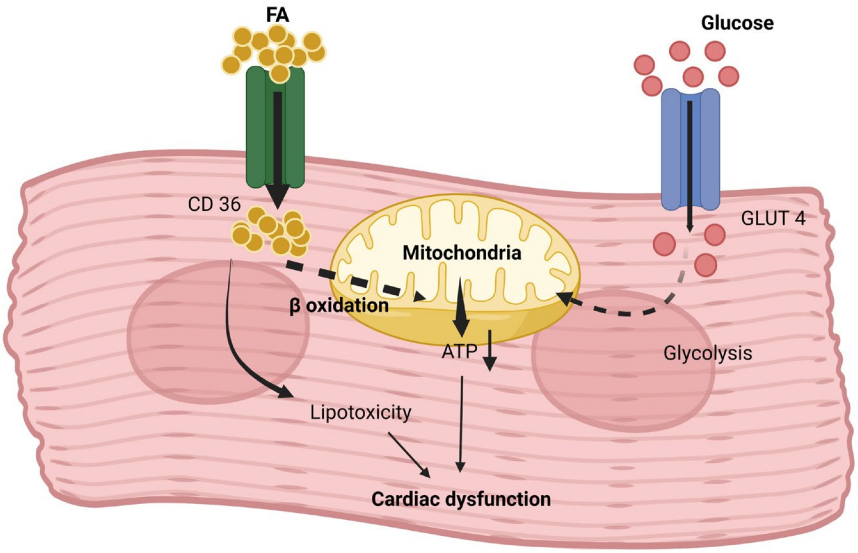

Obese cardiomyocyte

Figure 1.2: Schematic diagram of fat and glucose metabolism in the cardiomyocyte under healthy and obese conditions. A) Overview of major glucose and fatty acid metabolism pathways; B) Glucose and fatty acid use in the healthy (top) and obese cardiomyocyte (bottom).

1.2.1 Cardiac insulin signaling and insulin resistance

The translocation of the insulin-sensitive glucose transporter, GLUT4, to the sarcolemma accounts for the majority of glucose transport into cardiomyocytes[17]. During the fed state, insulin is released by the pancreatic β cells and stimulates insulin receptor signaling. Upon insulin binding to the alpha subunit of insulin receptor on the cardiomyocyte surface, β subunit conformation change occurs, and tyrosine kinase domains are activated. Insulin receptor tyrosine phosphorylation leads to the recruitment and tyrosine phosphorylation of insulin receptor substrate proteins (IRS1-IRS4). Phosphorylation of IRS1 or IRS2 activates PI3K/Akt signaling pathway.

Phosphorylated IRS proteins recruit and activate phosphatidylinositol 3-kinase (PI3K) enzymes. PI3K catalyzes the conversion of phosphatidylinositol 4,5-bisphosphate (PIP2) into phosphatidylinositol 3,4,5-trisphosphate (PIP3). PIP3 serves as a secondary messenger that recruits and activates protein kinase B (PKB or Akt). There are three isoforms of AKT (AKT 1, 2 and 3), of which AKT2 is central to insulin signaling. Phosphoinositide-dependent kinase 1 (PDK1) phosphorylates AKT at threonine 308. This phosphorylation partially activates AKT. Threonine 308 phosphorylation by PDK1 is necessary for AKT activation while serine 473 phosphorylation is crucial for full activation[18]. This latter phosphorylation is mediated by mammalian target of rapamycin complex 2 (mTORC2). Activated Akt promotes the translocation of GLUT4 from intracellular vesicles to the plasma membrane of cardiomyocytes[19]. This translocation allows for the uptake of glucose from the bloodstream into the cardiomyocytes, which can then undergo glycolysis to form pyruvate. Pyruvate can be transported into mitochondria for oxidation. Akt activation also stimulates glycogen synthesis[14]. Akt phosphorylates and inactivates glycogen synthase

kinase-3 (GSK-3), which is a negative regulator of glycogen synthesis. Inactivation of GSK-3 allows for increased glycogen synthesis and storage in cells through the activity of glycogen synthase[20].

During obesity, insulin signaling in the heart can become impaired, rendering the heart insulin resistant. Cardiac insulin resistance lowers the ability of the heart to use glucose as a fuel source and can promote cardiac dysfunction and heart failure. Insulin resistance in the heart is also associated with an increased risk of arrhythmias, oxidative stress, and cardiac remodeling[21].

1.3 Lysophosphatidic acid (LPA) metabolism and signalling

Increased circulating levels of the bioactive lipid, lysophosphatidic acid (LPA), have been implicated in obesity induced metabolic complications including insulin resistance, and cardiac dysfunction[19]. LPA is a simple glycerophospholipid that is composed of a glycerol backbone to which a single fatty acid and phosphate molecule are bound. LPA can be generated intra- or extracellularly and can function as a membrane lipid, glycerolipid intermediate, and signaling molecule. LPA is present in various biological fluids such as plasma, serum, and saliva[22]. Circulating LPA is generated by the secreted lysophospholipase D (lysoPLD), autotaxin (ATX), through the hydrolysis of lysophosphatidylcholine (LPC). ATX is also known as ectonucleotide pyrophosphatase/phosphodiesterase 2 (ENPP2)[17]. Circulating LPA levels are proportional to plasma ATX content and activity. For example, inhibiting plasma ATX activity by administrating PF-8380 reduced plasma LPA levels in mice *in vivo*. Reduction of circulating ATX levels by ~50% in heterozygous ATX knockout mice resulted in a ~50%

reduction in plasma LPA levels[18]. LPA binds to six GPCRs named as LPA 1 to 6 to stimulate intracellular signaling pathways involved in cell migration, proliferation, and growth. The signaling actions of LPA can be terminated by enzymatic dephosphorylation of LPA by lipid phosphate phosphatases (LPPs), converting LPA to monoacylglycerol (MAG)(Figure 1.3)[19]. The mammalian LPP family consists of three enzymes - LPP1 (PPAP2A), LPP2 (PPAP2C), and LPP3 (PPAP2B) - that are encoded by distinct genes (*PLPP1/PPAP2A*, *PLPP2/PPAP2C*, and *PLPP3/PPAP2B*, respectively). LPPs also catalyze the dephosphorylation of other extracellular and intracellular lipid substrates such as sphingosine-1-phosphate (S1P), ceramide-1-phosphate (C1P), diacylglycerol pyrophosphate, phosphatidic acid, and N-oleoylethanolamine phosphate[23,24].

1.3.1. Role of the autotaxin (ATX)-lysophosphatidic acid (LPA) axis in obesity and metabolic diseases

Data from murine models and humans point toward an increase in circulating LPA levels via upregulation of ATX secretion from adipocytes during obesity. HFD-fed male C57BL/6J mice had increased plasma LPA and adipose ATX mRNA levels[25]. In a small human cohort study, plasma LPA levels were positively correlated with BMI. Moreover, plasma LPA concentrations were higher in individuals who were obese compared to those with normal or underweight BMI[22]. In 3T3-L1 adipocytes, acute exposure to insulin enhances ATX activity in a PI3Kinase-dependent and mTORC1-independent manner, whereas prolonged exposure to insulin lowered ATX mRNA, protein, and activity. Glucose also increases ATX mRNA, protein, and activity in 3T3-L1 adipocytes in a time- and concentration-dependent manner[25]. It is plausible that hyperinsulinemia and hyperglycemia are underlying factors that increase ATX secretion from adipose tissue

during obesity and insulin resistance[18]. Also, LPA induces hypertrophy in cardiac myocytes, presumably through the stimulation of AKT and NF-κb signaling pathways[26]. Additionally, it has been suggested that LPA receptors 1 and 3 mediate left ventricular remodeling in rats subjected to myocardial infarction[26,27].

In a recent study from our lab, heterozygous whole body ATX knockout (ATX KO) mice fed high fat-high sucrose (HFHS) diet for 20 weeks showed reduced plasma ATX activity compared to WT mice (in contrast to the WT mice, HFHS feeding did not increase plasma ATX activity in the ATX KO mice), which was associated with improved glucose homeostasis and insulin signaling in perigonadal adipose tissue (PGAT), liver, skeletal muscle, and heart in ATX KO mice[18]. Another study using adipocyte specific ATX deficient mice showed that serum LPA and interstitial LPA levels were reduced by half after 10 weeks of HFD consumption compared to control. The same mice also showed smaller body weight gains[28]. Similarly, a prior study from our lab has shown that mRNA levels of LPA4-6 are increased in mice ventricles and cardiomyocytes during obesity[29]. The same study has also shown that LPA4 and LPA5 mRNA levels in human atrial tissue correlate with measures of obesity, suggesting that increased expression of distinct LPA receptors may promote enhanced LPA signaling in cardiomyocytes during obesity. Taken together, these data suggest that LPA contributes to the pathogenesis of obesity by promoting insulin resistance and impaired glucose homeostasis[29]. However, the mechanisms through which LPA affects distinct tissues including the heart during obesity remain unclear.

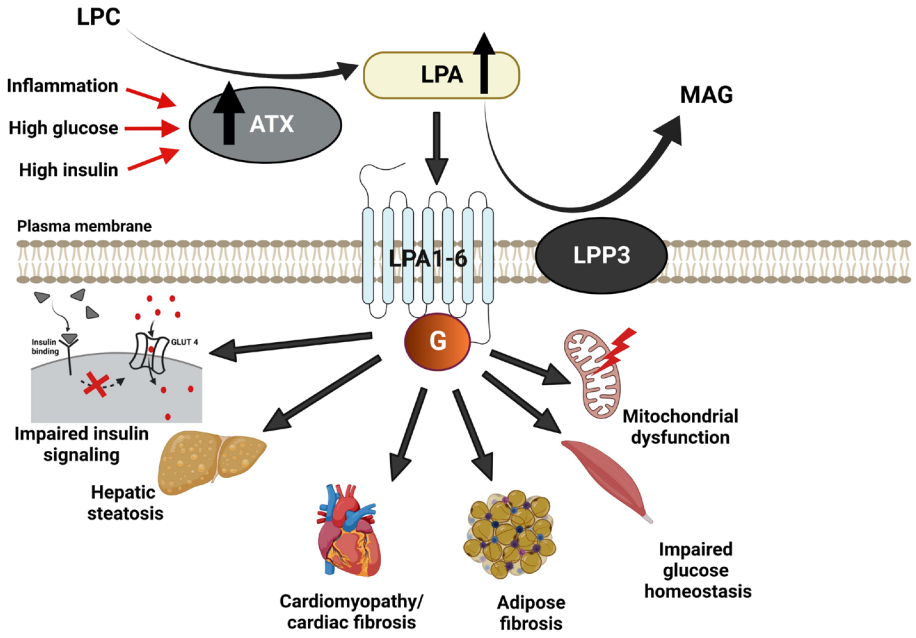

Figure 1.3: Schematic representation of LPA metabolism and metabolic effects of the ATX-LPA-LPP3 axis.
Image adapted from *Autotaxin-LPA-LPP3 Axis in Energy Metabolism and Metabolic Disease Int J Mol Sci. 2021 Sep 3;22(17):9575.*

1.4. Structure and Function of LPPs

LPPs contain six transmembrane α-helices. When located in the plasma membrane, the N- and C- termini face the cytoplasmic side and the three catalytic domains face the extracellular side, allowing LPPs to dephosphorylate substrates outside the cell. When LPPs are located in internal membranes, for example in the endoplasmic reticulum or Golgi, the active site is presumed to be facing the luminal surface of these organelles. LPPs also contain three extracellular/luminal loops. The enzymatic activity of LPPs is dependent on the N-glycosylated site located on the external loop localized between α- helices III and IV. This loop also harbors two of three catalytic domains, namely, C1 and C2. The third catalytic domain, C3, is located on the third loop between helices V and VI. C1 recognizes

substrate while C2 and C3 are involved in the phosphotransferase reaction as they contain the amino acids (histidine and arginine, respectively) needed for this reaction[24] There are three isoforms for LPPs, LPP1, LPP2 and LPP3. All three isoforms show similar catalytic activities but inactivation of the gene encoding for a specific LPP has demonstrated distinct biological effects of these enzymes[23,24]. For example, LPP1 deficiency led to a 50% increase in circulating LPA levels with no overt phenotypic manifestations shown at baseline, although glucose homeostasis and body weight were not reported in this study[30]. However, in transgenic mice with overexpression of LPP1, the concentration of circulating LPA was not significantly reduced[31]. Similarly, LPP2 knockout mice were viable and appeared to be normal[32]. In contrast to the deficiency of LPP1 and LPP2, global knockout of LPP3 in mice resulted in embryonic lethality due to failed development of embryonic vasculature[33]. The same study also demonstrated a 2.6-fold increase in LPA levels in the cultured media from embryonic fibroblasts of LPP3 knockout mice, suggesting that LPP3 is critical for extracellular LPA degradation[33]. In addition to its extracellular activity, LPP3 plays a role in the formation of retrograde transport carriers at the ER–Golgi interface and during its path to the plasma membrane as was identified in studies using HeLa cells[34].

1.5 Role of LPP3 in obesity and the heart

While numerous studies on LPP3 polymorphisms and mutant mouse models with LPP3 modulation in vascular cells have suggested that LPP3 upregulation protects from the development and complications of atherosclerosis and coronary artery disease, few studies have explored the role of LPP3 in obesity and associated metabolic and cardiovascular complications. Western diet-fed liver specific LPP3 knockout mice had increased plasma

LPA levels. In contrast, adipose specific LPP3 deficiency did not alter tissue LPA levels[35]. In smooth muscle cells, LPP3 has a protective effect. It was shown to reduce LPA stimulated Rho activation and smooth muscle cell migration[36]. A study using mice with cardiac-specific LPP3 deletion (CMLPP3−/−) showed that exogenously applied C17-LPA was degraded 6-fold more slowly in cardiomyocytes from CMLPP3-/- than control cells, highlighting the importance of cardiomyocyte LPP3 in regulating systemic LPA levels. The same study also showed markedly enhanced ERK and Rho activation, known downstream effectors of LPA receptor signaling, upon LPA stimulation in isolated neonatal cardiomyocytes from CMLPP3−/− mice. CMLPP3−/− mice had enlarged hearts indicative of cardiac hypertrophy and dysfunction, which was associated with progressive heart failure and premature mortality. Transmission electron micrograph analysis of the myocardium from CMLPP3-/- mice showed mitochondrial damage, and, in agreement with that, mitochondrial respiration was also significantly reduced in LPP3 deficient cardiomyocytes. However, it remains to be determined whether mitochondrial dysfunction in CMLPP3-/- mice is directly caused by LPP3 deficiency or a consequence of cardiac stress and heart failure in these mice[33]. Although these studies provide evidence that LPP3 mediates the degradation of extracellular LPA and is required for cardiac function, the role of LPP3 in myocardial mitochondrial metabolism and function during obesity remains unexplored.

1.6 Rationale and Objectives:

LPP3 has a major role in regulating circulating LPA levels[24,33,36]. LPP3 terminates LPA signaling by dephosphorylating LPA to MAG. Several studies have shown that plasma LPA levels are increased in obesity and that changes in LPA metabolism lead to cardiac insulin resistance and contractile dysfunction[23,24].

In my thesis, I hypothesized that overexpressing LPP3 specifically in cardiomyocytes protects the heart from metabolic and functional complications associated with diet-induced obesity. To elucidate the role of LPP3 in cardiac energy metabolism during healthy and obese conditions we generated cardiomyocyte specific LPP3 overexpressing mice and I aimed to:

1. Determine whether cardiac LPP3 overexpression alters plasma LPA levels.
2. Examine whether cardiac LPP3 overexpression has any impact on insulin sensitivity and mitochondrial respiration.
3. Determine whether cardiac LPP3 overexpression protects mice from obesity induced weight gain and cardiac dysfunction.
4. Assess whether LPP3 silencing in differentiated H9c2 cardiomyoblasts influences cell viability

CHAPTER 2: MATERIALS AND METHODS

2.1 Animal studies

2.1.1 Generation of cardiomyocyte-specific *Plpp3* overexpressing mice

Mice bearing *Lpp3*-floxed ($LPP3^{FL}$) alleles encoding for a CAG promoter driven *Plpp3* coding sequence (CDS) in reverse orientation in intron 1 of the ROSA26 locus were purchased from Cyagen (Santa Clara, CA). The expression of mouse *Plpp3* CDS is dependent on the expression of Cre recombinase, which removes a transcriptional stop provided by SV40 polyA sequence insertion between the CAG promoter and *Plpp3* CDS. $LPP3^{FL}$ mice were crossed with mice expressing Cre recombinase from the α myosin-heavy chain (Myh6) promoter to generate cardiomyocyte-specific LPP3 overexpressing mice ($LPP3^{OE}$). These mice were heterozygous for the *Lpp3*-floxed allele and hemizygous for the Cre recombinase. $LPP3^{FL}$ and Cre recombinase expressing mice were on the C57BL/6J background. Mice were housed on a 12 h light: 12 h dark cycle with *ad libitum* access to water and standard chow diet (Lab Diet, 5001) containing 30 kcal% protein , 13.5 kcal% fat and 58 kcal% carbohydrates (3.83 kcal% sucrose). All animal procedures were approved by the Dalhousie University Institutional Animal Care and Use Committee guidelines in accordance with the Canadian Council on Animal Care.

2.1.2 Genotyping of LPP3-floxed and cardiac specific LPP3 overexpressing mice

Genomic DNA was isolated from tissue collected from ear punches using DNA extraction reagent(Quanta Biosciences;95135-500). Tissue samples were submerged in 50 µl of

extraction reagents and heated at 95ºC for 30 min. Thereafter, samples were cooled to room temperature and 50 µl of stabilization buffer was added. The PCR reaction mix contained 6.25 µL of AccuStart II GelTrack PCR Supermix (Quanta Biosciences;95135-500), 0.5 µl of F4, R4, F5, R5, FCre and RCre, 1.1 µl of extracted DNA, and 2.15 µl of nuclease-free water. Primer sequences are summarized in Table 1. PCR products (WT- 607bp, $LPP3^{FL}$- 292 bp, Cre- 202 bp) were visualized using the Qiaxcel Advanced automated capillary electrophoresis system.

Table 1: Genotyping primer sequences.

Primer	Sequences 5′ to 3′
F4LPP3	CTT TAT TAG CCA GAA GTC AGA TGC
R4LPP3	TGC ATA GTG TTC TTC GTG TCC G
F5LPP3	AAG CAC GTT TCC GAC TTG AGT TG
R5LPP3	GGG TGA GCA TGT CTT TAA TCT ACC
FCreLPP3	GAA CGC ACT GAT TTC GAC CA
RCreLPP3	GCT AAC CAG CGT TTT CGT TC

2.2 Plasma LPA assay

Blood was collected in 10% EDTA coated microcentrifuge tubes and kept on ice for 30 min. Thereafter, blood was spun at 1,500 x g for 5 min at 4°C to obtain plasma. Immediately after plasma collection, 20 µl of 100 µM ATX inhibitor PF-8380 (Cayman chemicals, 12018) was added to 180 µl of plasma sample and plasma was kept on ice for

an additional 30 min[37]. Plasma LPA levels (50 µl of plasma per well) were measured using LPA ELISA kit from Aviva systems biology (OKCD2274) as per the manufacturer's instructions.

2.2.1 Preparation of ATX inhibitor

A 10 mM solution of the ATX inhibitor, PF-8380, was made by dissolving 5 mg of PF-8380 in 1.05 ml of DMSO. This stock solution was then diluted to a 100 µM sub stock solution, which was used to make a 10 µM working solution of PF-8380.

2.3 Insulin signaling study

For insulin signaling study *in vivo*, chow diet-fed 35-to-40 week-old female mice were injected intraperitoneally with 10 U of insulin (Humulin R, Eli Lilly) per kg body weight or an equal volume of saline following a 3-h food withdrawal. After 10 min, mice were euthanized by decapitation using a guillotine. Heart ventricles were collected and quickly frozen between two spatulas chilled in liquid nitrogen and stored at -80˚°C. Frozen hearts were powdered using mortar and pestle chilled in liquid nitrogen and homogenized in ice-cold lysis buffer containing (containing 20 mM Tris-HCl pH 7.4 (M151; VWR), 5 mM EDTA (4010; Calbiochem), 10 mM Na_4P_2O7 (P8010; Sigma), 100 mM NaF (S6521; Sigma), 1% Nonidet P-40 (I3021; Sigma), 2 mM Na_3VO_4 (567540; Millipore), protease inhibitor (P8340; 10 mg/ml; Sigma), and phosphatase inhibitor (524628; 10 mg/ml; Calbiochem)). Lysates were centrifuged at 1,200 x g for 30 min at 4°C and supernatants were transferred to another microcentrifuge tube. Protein concentration was determined using bicinchoninic acid (BCA) protein assay kit (23225; Thermo Fisher Scientific) according to the manufacturer's instructions. Protein samples (10-30µg) were diluted in 4X Laemmli Buffer with 1 mM

dithiothreitol (DTT) and boiled for 5 min at 100°C. Lysates were stored at -80°C until further biochemical analysis.

2.4 Mitochondrial respiration study

Respiratory oxygen flux in permeabilized myofibers was measured in high-resolution using the Oxygraph-2k (OROBOROS Instruments), which measures the oxygen flux changes following the addition of different substrates of mitochondrial respiration. Small heart tissue was incubated in ice cold biopsy preservation solution (BIOPS, 10 mM Ca^{2+}-EGTA buffer, 0.1 µM free Ca^{2+}, 20 mM imidazole, 20 mM taurine, 50 mM K-MES, 0.5 mM DTT, 6.56 mM $MgCl_2$, 5.77 mM ATP, 15 mM phosphocreatine, pH 7.1, Table 2). Excess connective tissue, fat, and tendons were removed, and fiber bundles were mechanically separated using forceps. Fiber bundles were permeabilized in 2 ml of BIOPS containing 50 µg/ml saponin and gently agitated on ice for 30 min. Thereafter, fiber bundles were washed in mitochondrial respiration medium (MiR05) buffer (0.5 mM EGTA, 3 mM $MgCl_2$-$6H_20$, 60 mM lactobionic acid, 20 mM taurine, 10 mM KH_2PO_4, 20 mM 135, HEPES, 110 mM sucrose and 1 g/L FAF-BSA, Table 3), fiber wet weights obtained, and samples were placed in the Oxygraph chambers. Samples were assessed in 2 ml hyper-oxygenated MiR05 buffer at 37°C, and reoxygenated as necessary throughout the protocol. Instrumental background O_2 consumption was corrected using equations determined under the same parameters used for experimental data collection. Respiration and glucose oxidation was estimated after sequential addition of malate, pyruvate, and adenosine diphosphate (ADP). Details of the addition and titration of substrates and inhibitors are listed in Table 4. Mitochondrial respiration was normalized to wet tissue weight of permeabilized fibers.

Table 2: Chemical components, concentrations, and vendor information for component of BIOPS buffer.

Chemical Compound	Concentration	Vendor; Catalog Number
CaK_2EGTA	2.77 mM	NA
K_2EGTA	7.23 mM	NA
Na_2ATP	5.77 mM	Sigma; 2383
$MgCl_2.6\ H_2O$	6.56 mM	Scharlau; MA0036
Taurine	20 mM	Sigma; T 0625
Na_2Phosphocreatine	15 mM	Sigma; P 7936
Imidazole	20 mM	Fluka; 56750
Dithiothreitol (DTT)	0.5 mM	Sigma; D 0632
MES hydrate	50 mM	Sigma; M8250

Table 3: Chemical components, concentrations, and vendor information for components of mitochondrial respiration medium (MiR05) buffer.

Chemical Compound	Concentration	Vendor; Catalog Number
EGTA	0.5 mM	Sigma; E4378
$MgCl_2.6\ H_2O$	3 mM	Scharlau; MA0036
Lactobionic acid	60 mM	Sigma; 153516
Taurine	20 mM	Sigma; T0625
KH_2PO_4	10 mM	Merck; 104873
HEPES	20 mM	Sigma; H7523
Sucrose	110 mM	Sigma; 84097
Fatty acid-free-BSA	1 g/l	Sigma; A6003

Table 4: Sequence of addition of substrates and inhibitors for mitochondrial respiration analysis. Fatty-acid linked respiration was performed following addition of palmitoyl-carnitine/octanoyl-carnitine

Chemical	Concentration	Mark	Vendor; Catalog number
Malate	0.5 mM	M	Sigma; M1000
Pyruvate/**Palmitoyl-carnitine**	5 mM/ 50 µM	Pyr	Sigma; P5280
ADP	0.1 mM	D 0.1	Sigma; A2754
ADP	0.5 mM	D 0.5	Sigma; A2754
ADP	5 mM	D 5	Sigma; A2754
Octanoyl- Carnitine	0.2 mM	OCT	APExBIO Technology; B6371
FCCP	0.5 µM	FCCP	Sigma; C2920
Rotenone	0.5 µM	R	Sigma; R8875
Succinate	10 µM	S	Sigma; S3674
Antimycin A	5 µM	AmA	Sigma; A8674

2.5 Diet-induced obesity studies

Ten to eleven week-old male and female heterozygous $LPP3^{OE}$ and $LPP3^{FL}$ mice were randomly assigned to groups fed either a low fat diet containing 10% kcal fat or a high fat diet containing 60% kcal fat and water for 22 weeks (Table 5). Body weight was recorded monthly, and body weight gain was quantified as fold change by dividing the monthly body weight by the starting body weight for each mouse. Mice were subjected to glucose tolerance test (GTT) at 8 weeks and insulin tolerance test (ITT) at 11 weeks post diet start. Peripheral fat accumulation in isoflurane-anesthetized mice was determined by X-ray imaging using a Bruker In-Vivo Xtreme imager, 19 weeks after diet start. Planar X-ray images were analyzed using ImageJ software and area of peripheral fat was expressed as percent of total body area. Cardiac function analysis was performed using a Doppler flow velocity system. The E/A ratio, IVCT, IVRT, and heart rate were the parameters assessed to determine cardiac functioning. Mice were euthanized by decapitation following a 16 h food withdrawal period, and tissues were collected and stored at -80°C. Perigonadal adipose tissue (PGAT) and the liver were weighed prior to being flash-frozen.

Table 5: Diet composition

(DIO) Formulas	Low fat diet	Chow diet	High fat diet
Product #	Research Diet D12450J	Lab Diet, 5001	Research Diet D12450J
	kcal%	kcal%	kcal%
Protein	20	30	20
Carbohydrate	70	58	20
Fat	10	13.5	60

2.5.1 GTT and ITT

Blood glucose was measured using a One Touch Verio Reflect blood glucose meter. For GTT, 16-h fasted awake mice were injected intraperitoneally with 20% (w/v) D-glucose at 2 mg/kg body weight or an equal volume of saline. For ITT, awake mice were injected intraperitoneally with 1 U human insulin (Humulin R, Eli Lilly) per kg body weight or an equal volume of saline following a 4-h food withdrawal. After injection, blood glucose was determined at the times indicated.

2.5.2 Cardiac function analysis

Cardiac function was assessed using pulsed wave doppler flow velocity system (Indus instruments). LFD or HFD fed male and female mice were anesthetized with 2% isoflurane in oxygen and placed in a supine position on a 37ºC platform of the Rodent surgical monitoring (RSM) system. Once anesthetized, isoflurane level was reduced to 1-1.5%. Animal was secured to the electrodes on the RSM. The ECG wave form is recorded from the RSM. The hair on the animal was removed by shaving if required. A small amount of water is used between the probe tip and the skin surface to obtain a good acoustic coupling. 10Hz doppler probe (Indus Instruments Doppler Flow Velocity System, made by Indus Instruments 721 Tristar Drive Webster, Texas, 77598, USA) tip was placed just below the xiphoid process and aimed toward the right ear to get the mitral inflow velocity signal. Probe tip was pointed toward to the left ear to get the aortic outflow signal. Mitral inflow velocity signal represents the flow from the left atrium into the left ventricle during the diastolic phase of the cardiac cycle. The mitral flow velocity signal consists of two flow peaks; one is an early (E) peak that occurs during rapid filling phase, the other occurs during the atrial (A) filling phase. Mitral inflow- derived parameters include E/A ratio,

Isovolumic contraction time (IVCT) and Isovolumic relaxation time (IVRT). IVCT represents the time interval from the closure of the mitral valve to the opening of the aortic valve. It is an excellent measure of contraction. IVRT represents the time interval from the closure of the aortic valve to the opening of the mitral valve and it is a measure of relaxation. Aortic outflow velocity signal is the result of myocardial contraction, leading to the systolic ejection of the blood within the left ventricle. Aortic peak velocity was derived from the aortic outflow signal and represents the peak velocity of the aortic outflow.

2.6 Cell culture

2.6.1 H9c2 cell culture

Female H9c2 rat embryonic cardiomyoblasts (H9c2(2-1), ATCC CRL-1446) were cultured at a density of 5 x 10^5 cells per 35 mm plate and maintained in Dulbecco's modified Eagle's medium (DMEM) containing 5 mM glucose (SH30243.01; DMEM-HG; Hyclone Laboratories, UT, USA) and supplemented with 10% fetal bovine serum (FBS) (FBS; 12483020; Gibco) at 37°C and 5% CO_2 until 90% confluency. Cells were then differentiated in DMEM (11966025; Thermo Fisher Scientific, MA, USA) supplemented with 0.5% FBS and 5 mM glucose (0188; Amresco) for 48 h. After differentiation, cells were used for different treatments as indicated. Cells were harvested in phosphate buffered saline (PBS) and centrifuged at 10,000 x g for 10 min at 4°C. Cell pellets were sonicated in lysis buffer and centrifuged at 10,000 x g for 10 min. The supernatant was transferred to another microcentrifuge tube and protein concentration was determined using the BCA assay kit. Lysates were stored at -80°C for subsequent immunoblot analysis.

2.6.2 Adult mouse cardiomyocyte isolation and culture

Adult cardiomyocytes were isolated from hearts of 30 to 32 week-old LPP3^{FL} or LPP3 ^{OE} mice fed chow diet. Hearts were excised and washed in ice-cold perfusion buffer (pH 7.4) (Table 6) containing NaCl (113 mM), KCl (4.7 mM), KH_2PO_4 (0.6 mM), Na_2HPO_4 (0.6 mM), $MgSO_4$ •$7H_2O$ (1.2 mM), $NaHCO_3$ (12 mM), HEPES (10 mM), taurine (30 mM), 2,3 butandione monoxime (BDM, 10 mM), and glucose (5.5 mM). Hearts were then perfused in Langendorff mode with calcium-free perfusion buffer at a flow rate of 4 ml/min for 6 min until the effluents became clear, followed by perfusion with collagenase (1.6 mg/ml, Worthington Lot: 45D15719)-containing digestion buffer (Table 6) for 20-25 min. After collagenase digestion, hearts were removed from the rig and placed in a 60 mm dish. 10 ml of stopping buffer (Table 6) was added to the dish to stop digestion and hearts were minced into small pieces using fine scissors. Collagenase buffer was collected from the rig and used to make a suspension of the minced heart. This suspension was passed through a 100 μm filter to further dissociate the tissue and transferred to a 50 ml centrifuge tube. Suspension volume was adjusted to 30 ml. The cell suspension was spun to pellet the cells at 500 x g for 45 s and the supernatant was decanted. Cells were then made calcium-tolerant by resuspending the cell pellet in stopping buffers, C1, C2, and C3, with increasing $CaCl_2$ concentration (C1:100 μM, C2:400 μM and C3:900 μM, Table 6). Cells were incubated in each solution for 10 min in a water bath at 37˚°C. After each incubation, viable cells settled to the bottom of the centrifuge tube and the supernatant was removed using a Pasteur pipette, followed by the addition of the next calcium solution with higher concentration. Following incubation with C3, the supernatant was removed, and 1 ml of plating medium was added to resuspend and count cells. Cells were seeded at 25,000-50,000 cells on

laminin-coated 25 mm x 25 mm slides or 35 mm plates and were incubated in plating medium (Table 6) for 2 h for recovery before cells were used for experiments. Cells were then harvested in PBS, followed by centrifugation to pellet the cells at 10,000 x g for 10 min at 4°C. Cell pellets were sonicated in lysis buffer on ice, followed by centrifugation at 10,000 g for 10 min at 4˚C. The supernatant was transferred to another microfuge tube and protein concentration was determined using the BCA protein assay kit. Lysates were stored at -80˚°C for subsequent analysis.

Table 6: AMCM buffer and media composition.

Digestion Buffer	**Amount**	**Final Conc.**	**Volume**
Perfusion Buffer	------	------	50 ml
Collagenase II	75 mg	2.4 mg/ml	------
Calcium chloride	100 mM	12.5 µM	6.25 µl

Stopping Buffer:	**Stock**	**Final Conc.**	**Volume**
Perfusion Buffer	------	------	36 ml
Calf Serum		2.4 mg/ml	4 ml
Calcium Chloride	100 mM	50 µM	20µL

	C1	**C2**	**C3**
Stopping Buffer	10 mL	10 mL	10 mL
Calcium Chloride (100 mM stock)	10 µL (100 µM)	40 µL (400 µM)	90 µL (900 µM)

MEM HBSS:	**g/L**	**20 ml**	**50 ml**
MEM HBSS	107 g	0.214 g	0.535 g
Sodium Bicarbonate	0.35 g	0.007 g	0.0175 g
Adjust pH to 7.3 and equilibrate for 2-3 h in incubator at 37°C and 5% carbon dioxide			

Plating Medium	**Stock**	**Final Conc.**	**Volume**
MEM HBSS	------	------	43.5 ml
Calf Serum	100 %	10%	5 ml
BDM		10 mM	0.01 g
Penstrep			0.005 g
Taurine	500 mM	5 mM	0.5 ml
Carnitine	500 mM	2 mM	0.2 ml

2.6.3 Fatty acid treatments

Sodium palmitate (P9767; Sigma) and Sodium oleate (07501; Sigma) was complexed to fatty acid free BSA in DMEM. A 100 mM palmitate or oleate stock solution was made by adding 27.841 mg of sodium palmitate or 30.444 mg of sodium oleate to 1 ml of DMEM and warmed to 100°C to dissolve completely. The 100 mM stock solution was diluted in 1% fatty acid free BSA in DMEM to desired concentration for cell incubation. Media was sterile filtered prior to cell incubation.

2.6.4 *Lpp3* knockdown using siRNA

H9C2 cells were cultured as described in section 2.6.1. Differentiated H9C2 cells were transfected with 10 nM control siRNA (silencer negative control) or *Lpp3* targeting siRNA (siLPP3) using RNAiMAX transfection reagent and OptiMEM for 48 h. siRNA (siRNA negative control: Thermo,4390844; siLPP3: Thermo, S140505) was diluted in Opti-MEM (31985062; Life Technologies) and added to Lipofectamine RNAiMAX (13778150; Life Technologies), resulting in a complex with 4 or 6 µl of Lipofectamine and a final concentration of 10 or 15 nM of siRNA per plate, as indicated in figure legends. The siRNA: lipofectamine solution was prepared in sterile 5mL tubes and incubated for 15-20 min at room temperature to aid complexation. Subsequently, media on plates was replaced with 2.75 ml of the cells differentiation media. 250 ml of the siRNA: lipid complex was added dropwise to the appropriate plates, and then cells were incubated 48 h with the siRNA complex before cell harvest or additional treatment. Cells were harvested after 48 h transfection. Harvested cells were centrifuged at 10,000 x g for 10 min and cell pellets were stored at -80°C for future use.

2.7 Quantitative polymerase chain reaction

RNA was extracted from samples (H9C2 cells, tissues, AMCMs) using RiboZol and chloroform. For the phenol-chloroform method using RiboZol RNA extraction reagent (VWRVN580; VWR), cell pellets or tissues were resuspended in 750 µl and 500 µl of RiboZol in RNase/DNase free tubes respectively. Samples were sonicated for 30 sec, before 350 µl of chloroform (613312; Sigma Aldrich) was added. Samples were inverted by hand 5-10 times, and incubated at room temperature for 3 min until two separate layers were indistinguishable. Samples were centrifuged at 12,000 x g for 20 min at 4°C to separate phases. The upper aqueous phase was transferred to a fresh RNase/DNase-free tube, while the lower phase and interphase were discarded. This was followed by a second extraction with an additional 100 µl of chloroform added to the upper phase. Samples were again inverted and incubated at room temperature before another centrifugation at 12,000 x g for 20 min at 4°C. Again, the upper phase was transferred to a fresh RNase/DNase-free tube, and the lower phase and interphases were discarded. Ice-cold 100% isopropanol (500 µl; Sigma-Aldrich) was added to the aqueous phase, and the tubes were inverted by hand before incubation at room temperature for 10 min. Samples were centrifuged at 12,000 x g for 20 min at 4°C to pellet the RNA. The supernatant was discarded, and the RNA pellet was then rinsed and resuspended in 1 ml ice-cold 75% ethanol prepared in nuclease-free water (10977-015; Life Technologies). Samples were briefly vortexed and then centrifuged at 7,500 x g for 5 min at 4°C. The ethanol wash was discarded, and the RNA pellet was left to air dry for 30 min as per the manufacturer's instructions. RNA was resuspended in nuclease free water. The quality and quantity of RNA was assessed using Nanodrop method (Synergy hybrid reader- GEN 5 2.09).

cDNA was synthesized using qScript cDNA SuperMix (95048; Quantabio) from 500 ng of RNA. qPCR reactions were carried out in 96-well plates on a ViiA7 real-time PCR machine and contained 2 µl of cDNA template, 5 µl of SYBR green Low ROX PCR super mix, 0.25 µM for each forward and reverse primer, and nuclease free water in a total of 10 µl per reaction. Primer sequences are summarized in Table 7. *Lpp3* mRNA levels were determined using qBase+ software and normalized to two reference genes specific for each sample type. Reference gene pairs were selected based on methodology as previously reported[38]. *Lpp3* mRNA levels were presented as fold change compared to control.

Table 7: Sequences of mouse and rat primers for qPCR.

Primer	Sequences 5' to 3'
rB2M-F	ACATCCTGGCTCACACTGAA
rB2M-R	ATGTCTCGGTCCCAGGTG
rGAPDH-F	GGCCGAGGGCCCACTA
rGAPDH-R	TGTTGAAGTCACAGGAGACAACCT
mHPRT1-F	CAGTCCCAGCGTCGTGATTA
mHPRT1-R	GGCCTCCCATCTCCTTCATG
mRpl27 -F	AAGCCGTCATCGTGAAGAACA
mRpl27 -R	CTTGATCTTGGATCGCTTGGC
mPPAP2B- F	ACAAGCACCATTAAGCCTTACCG
mPPAP2B-R	ATCCCCACCGCACAGAGCA
rPPAP2B-F	CCACTCGCAAACTTCAGCAC
rPPAP2B-R	CCAAATCCCGAGCAGGAACT

2.8 Immunoblotting analysis

Samples were homogenized in lysis buffer (20 mM Tris-HCl pH 7.5, 5 mM EDTA, 10 mM $Na_4P_2O_7$, 100 mM NaF, 1% NP-40) containing 2 mM sodium orthovanadate, 2 mM protease inhibitor cocktail, and 100 µg/ml phosphatase inhibitor cocktail on ice using a sonicator. Protein concentrations of tissue and cell lysates were quantified colorimetrically using a BCA protein assay kit. Lysates were subjected to SDS-PAGE or by pre-cast CriterionTM TGXTM 4-20% acrylamide gradient gels (5671095; Bio-Rad) and proteins were transferred to a nitrocellulose membrane (0.2 µM; 1620112; Biorad). Following the transfer, membranes were rinsed in ddH2O and stained with the Pierce Reversible Protein Stain Kit (24580; Thermo Fisher Scientific) to assess loading and transfer efficiency. Membranes were imaged using a ChemiDoc MP Imaging system, and the stain was removed using Pierce Stain Eraser. Membranes were blocked for 1 h in tris-buffered saline (TBS) with 0.05% Tween-20 (0777; VWR) (TBS-T) containing 5% (w/v) skim milk and incubated overnight at 4°C with primary antibodies. Primary antibodies (1% milk-TBS-T with sodium azide) are summarized in Table 8. Membranes were incubated with horseradish peroxidase (HRP)-tagged anti-mouse or anti-rabbit secondary antibody diluted in 5% milk-TBS-T for 2 h at room temperature. Immunoblots were developed using the Western Lightning Plus chemiluminescent substrate (NEL103E001EA; PerkinElmer) or Clarity™ Western Enhanced Chemiluminescence Substrate (1705060S; BioRad) Western Lightning Plus-ECL enhanced chemiluminescence substrate. To strip the protein from the blots prior to re-probing, membranes were incubated in 50 mL of 0.5M Tris-HCl/SDS buffer supplemented with 250 µl β-mercaptoethanol (6010; OmniPur®) for 1 h at 50°C. Densitometric analysis was performed using Image lab software v6.1 (Bio-Rad). Protein

levels were corrected to protein stain. Phosphorylated protein levels were normalized to total protein levels and expressed as a ratio of phosphorylated protein/total protein.

Table 8: List of antibodies used for immunoblot analysis.

Target	Company	Catalog number
pAKT Ser473	Cell Signaling	9271
AKT1	Millipore	05-591
pAKT Thr308	Cell Signaling	4056
P70S6K	Cell Signaling	2708
pP70S6K Thr389	Cell Signaling	9234
LPP3	Novus biologicals	NBP257350
Anti-rabbit secondary	Cell Signaling	7074

2.9 Statistical analysis

Statistical analysis was performed using GraphPad Prism software version 9. Results are expressed as mean ± standard error of the mean (SEM). Comparisons between multiple groups were performed using a one-way or two-way analysis of variance (ANOVA) followed by a Tukey or Sidak multiple comparison test, as appropriate. Unpaired two-tailed Student's t-tests were also performed where indicated. P-values of less than 0.05 were considered statistically significant.

CHAPTER 3: RESULTS

3.1 Tissue LPP3 levels and plasma LPA concentrations in mice with cardiomyocyte-specific LPP3 overexpression

To provide evidence that LPP3 is overexpressed in the heart, LPP3 protein levels were assessed in liver, heart, brown adipose tissue (BAT), and soleus muscle from chow diet fed 35 to 40 week-old male and female $LPP3^{FL}$ mice (body weight (mean ± S.E.M.)- male: 28.93 ± 1.55, female: 23.46 ± 0.95) and $LPP3^{OE}$ mice (body weight (mean ± S.E.M.)- male: 31.19 ± 1.26, female: 24.33 ± 1.43). In both male and female $LPP3^{FL}$ mice, LPP3 protein levels were highest in the liver and lowest in the heart (Fig. 3.1 A to D). Cardiac LPP3 protein content in the heart was increased by ~37-fold in male and ~49-fold female $LPP3^{OE}$ mice compared to $LPP3^{FL}$ mice (Fig. 3.1 A to D). The enzymatic activity of LPP3 depends on the N-glycosylated site on the external loop. There are two bands detected for LPP3 in the western blot, which are of 25and 37KDa size. The higher molecular weight band (37KDa) is believed to be the glycosylated form or LPP3 Consistent with increased cardiac protein expression in $LPP3^{OE}$ mice, *Lpp3* mRNA levels were increased 8-fold in cardiomyocytes isolated from male (Figure.3.1 E) and female $LPP3^{OE}$ mice compared to control (Figure. 3.1 G). Since LPP3 degrades circulating LPA and converts it to MAG, the LPA concentration in blood plasma from control and LPP3 overexpressing mice was determined using a competitive ELISA kit (Fig. 3.1 F, H). Plasma LPA levels were reduced by 41% in male and 57% in female $LPP3^{OE}$ mice when compared to the control group, suggesting that cardiomyocyte-specific LPP3 overexpression reduces circulating LPA levels in chow-fed mice (male and female). These data show that LPP3 is substantially and

specifically elevated in the heart/cardiomyocytes from LPP3^{OE} mice, which is sufficient to lower circulating LPA levels at baseline.

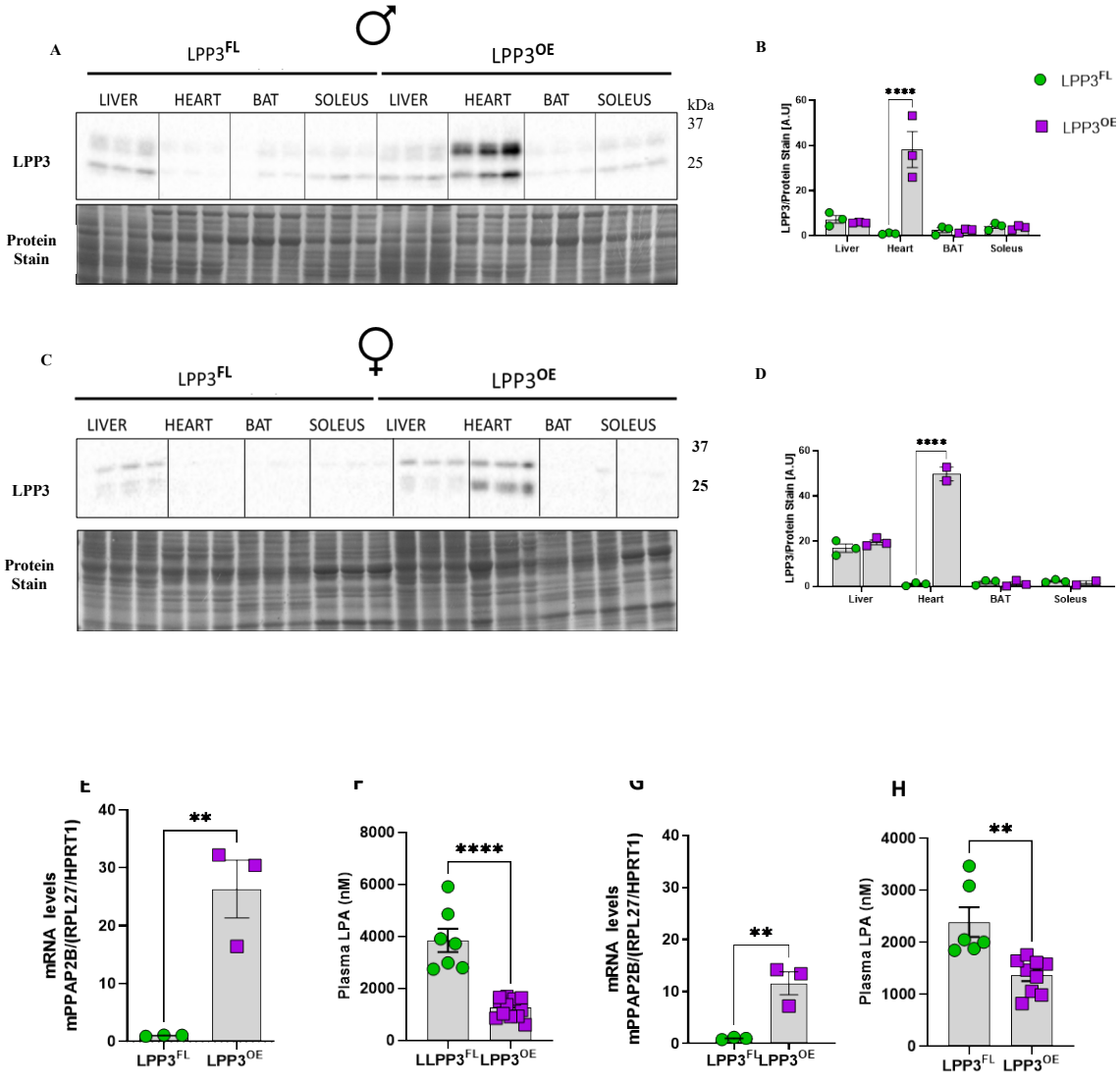

Figure 3.1. Cardiac specific LPP3 overexpression reduces plasma LPA levels. 35- 40-week-old male and female chow diet fed mice were fasted for 16 h and 4 h, respectively. LPP3 protein levels were measured in indicated tissues by immunoblot analysis. Plasma LPA levels were measured using a competitive ELISA kit. A) Tissue immunoblot from male mice and B) densitometric analysis of LPP3 protein. C) Tissue immunoblot from female mice and D) densitometric analysis of LPP3 protein. E) Cardiomyocyte *Lpp3* mRNA levels from male mice. F) Plasma LPA levels in male mice. G) Cardiomyocyte *Lpp3* mRNA levels from female mice. H) Plasma LPA levels in female mice. Data are expressed as mean ± S.E.M. LPP3 protein levels were corrected to protein stain. mRNA expression is normalized to indicated reference genes. Statistical analysis was performed using two-way ANOVA (B & D) with Tukey's with multiple comparison or unpaired t test (E,F,G,H); n = 3 (A,B,C,D); n =3 (E&G), n= 6-14 (F&H); $^{**}p< 0.01$, $^{****}p<0.0001$.

3.2 Mitochondrial substrate metabolism in myofibers from chow diet-fed LPP3^{OE} mice

Previous studies from our lab and others have shown that increased LPA levels can impair mitochondrial substrate metabolism and increase ROS production[18]. We next wanted to determine whether cardiac mitochondrial respiration was altered by LPP3 overexpression and reduced circulating LPA levels. Permeabilized myofibers from 16-h fasted chow diet-fed male mice were examined for pyruvate (Pyr)- and palmitoyl carnitine (PC)-linked respiration using physiological, non-saturating concentrations of ADP (up to 0.5 mM). During Pyr-linked respiration, myofibers from LPP3^{OE} mice showed a significant increase in respiratory oxygen consumption following the addition of ADP (complex I-linked respiration) and rotenone-succinate (complex II-linked respiration) compared with the control group (Fig. 3.2 A). Uncoupled respiration (using FCCP) was also significantly increased in LPP3^{OE} mice (Fig. 3.2 B). Mitochondrial respiration upon incubation with fatty acyl-carnitines was comparable between genotypes (Fig 3.2 C,D). Together, these data suggest that overexpression of LPP3 in cardiomyocytes enhances mitochondrial Pyr-linked respiration in the heart.

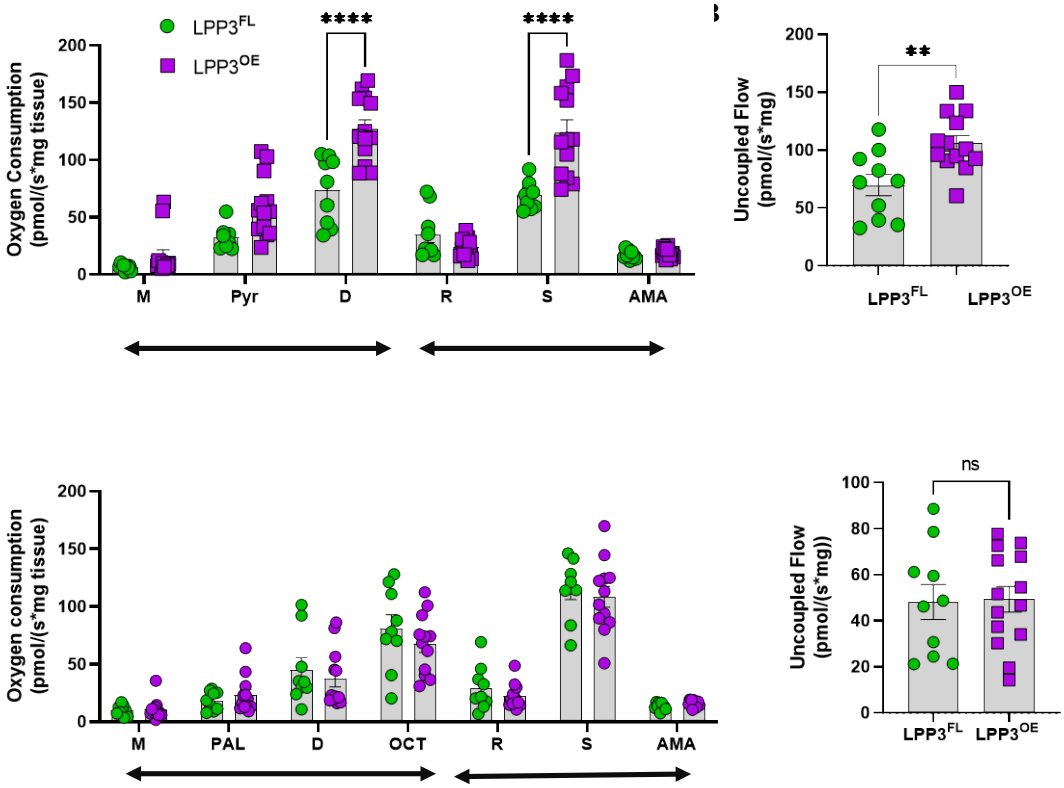
LPP3FL
LPP3OE
Oxygen Consumption (pmol/(s*mg tissue)
****
****
M
Pyr
D
R
S
AMA
Uncoupled Flow (pmol/(s*mg)
**
LPP3FL
LPP3OE
Oxygen consumption (pmol/(s*mg tissue)
M
PAL
D
OCT
R
S
AMA
Uncoupled Flow (pmol/(s*mg))
ns
LPP3FL
LPP3OE

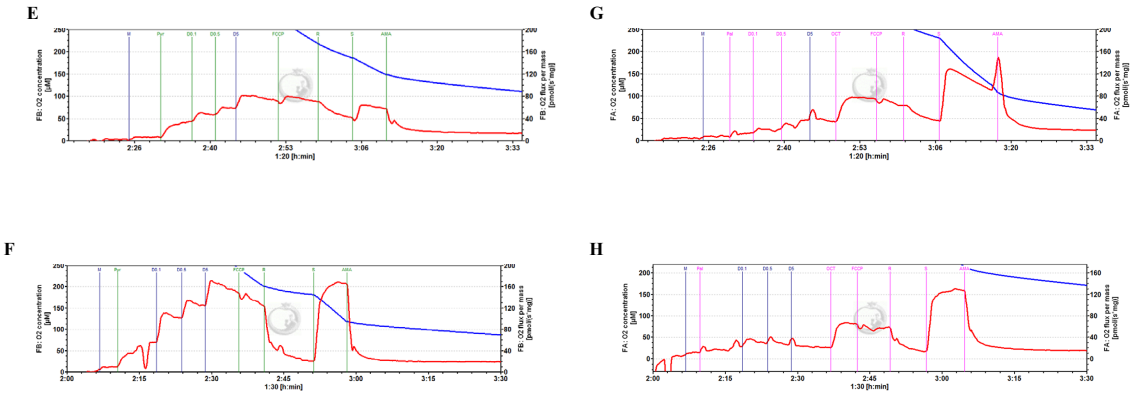
E
G
F
H

Figure 3.2. Mitochondrial Pyr-linked respiration is increased in the heart from LPP3^{OE} mice. Heart muscle fibers from male 35–40-week-old chow diet fed control and LPP3^{OE} mice were subjected to mitochondrial respiration analysis. A) Pyr-linked respiration and B) uncoupled flow during pyruvate-linked respiration; C) Fatty acylcarnitine-linked respiration and D) uncoupled flow during fatty acylcarnitine-linked respiration E) Representative trace of Pyr-linked respiration from control (LPP3^{FL}) mice and F) LPP3^{OE} mice. G) Representative trace of fatty acylcarnitine respiration from control (LPP3^{FL}) mice and H) LPP3^{OE} mice . Values are corrected to tissue weight and the oxygen consumption rate following the addition of AMA. Graphs represent mean ± S.E.M. Statistical analysis were performed using two-away ANOVA (A & C) and unpaired t-test (B & D), $^{**}p<0.01$, $^{****}p<0.0001$. All data are from two independent experiments with n = 10-14 biological replicates in each trial.

3.3 In vivo insulin signaling in the heart from chow-fed LPP3^{OE} mice

Prior studies from our lab have shown that incubation with LPA impairs insulin signaling in C2C12 myotubes[18] and H9C2 cells (unpublished data). To determine whether cardiac-specific LPP3 OE and the corresponding reduction in circulating LPA levels has any effect on cardiac insulin signaling at baseline, we performed an in vivo insulin signaling analysis in our mouse model. Insulin stimulated AKT phosphorylation at S473 and T308 was comparable between LPP3^{OE} and control mice (Fig 3.3 A,B,C). P70S6K phosphorylation at T308 which is downstream of AKT was also comparable between the genotypes (Fig. 3.3 A, D). Taken together, these data suggest that overexpression of LPP3 in the heart and a reduction of circulatory LPA levels does not alter cardiac insulin signaling at baseline.

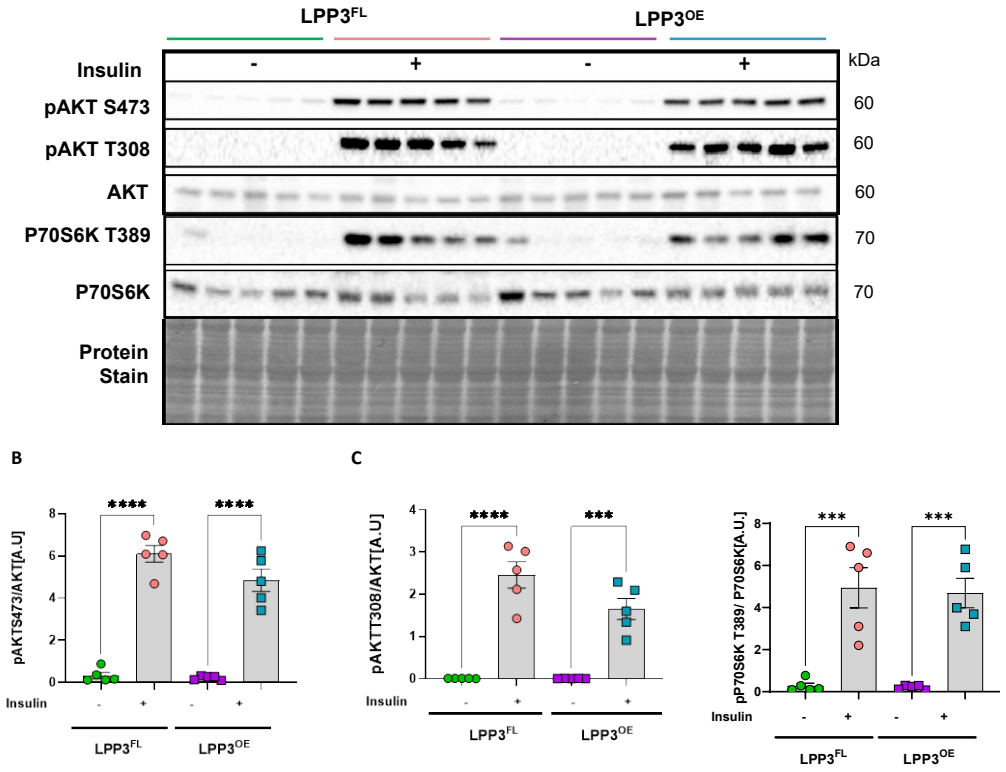

Figure 3.3. LPP3 overexpression in the heart does not alter cardiac insulin signaling at baseline. Female chow diet-fed 35-40 week old control and LPP3^{OE} female mice were injected with 10U/kg of insulin or equal volume of saline following a 4-h food withdrawal and insulin signaling in the heart was examined by immunoblot analysis. A) Immunoblot and densitometric analysis of AKT phosphorylation at B) S473 and C) T308 corrected to total AKT and D) p70s6k phosphorylation at T389 corrected to total p70s6k (n=5). Data are presented as mean ± s.e.m. Statistical analysis was performed using one-way ANOVA followed by Tukey's multiple comparison test. ***p<0.001, ****p<0.0001. A.U arbitrary unit.

3.4 Diet Studies

To clarify the role of cardiac LPP3 in glucose homeostasis and cardiac function at baseline and following diet-induced obesity, we fed male and female $LPP3^{FL}$ and $LPP3^{OE}$ mice LFD or HFD for 20 weeks. Mice were subjected to body weight measurements every four weeks and a GTT and ITT at the 8^{th} and 11^{th} week, respectively, to assess systemic glucose homeostasis. Peripheral fat accumulation and cardiac function were determined at the 19^{th} week post-diet start. Following euthanasia, PGAT and ventricle weight, and plasma LPA levels were determined.

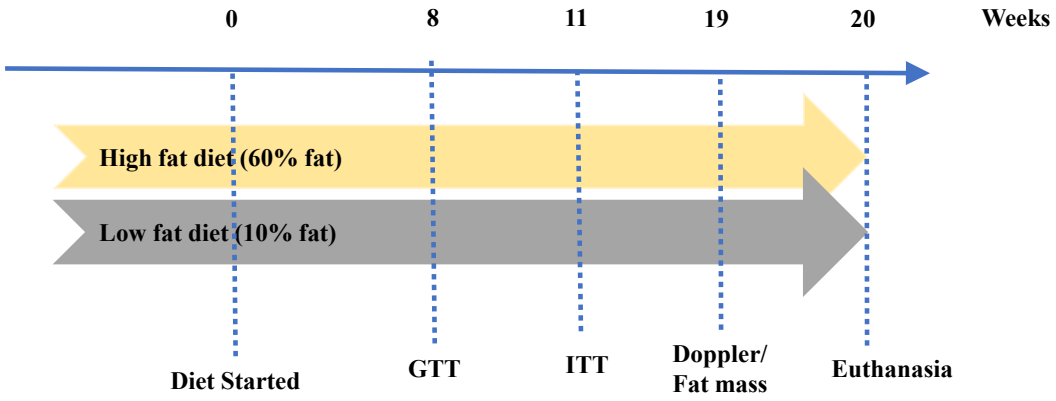

Figure 3.4. Timeline of procedures conducted during the HFD feeding study.

3.5 Female LPP3^{OE} mice are protected from a HFD-induced increase in plasma LPA concentration

Several studies have shown that feeding mice with an obesogenic diet results in increased circulating LPA levels[28]. In humans, a recent study showed that plasma LPA correlates with BMI[22]. These studies suggest that the consumption of a fat-rich diet leads to increased circulating LPA levels. Also, a recent study using cardiomyocyte specific LPP3 knockout male mice showed diminished LPP activity in cardiomyocytes and markedly increased plasma LPA levels, suggesting that cardiomyocyte LPP3 plays an important role in regulating circulating LPA levels[33].

From our earlier studies we understood that cardiomyocyte-specific LPP3 overexpression reduces plasma LPA levels in both chow diet-fed male and female mice at baseline. Interestingly, HFD feeding led to a ~58% increase in plasma LPA levels in female LPP3^{FL} mice compared to LFD-fed mice while only a trend towards increased LPA levels was observed in male HFD-fed LPP3^{FL} mice. Moreover, HFD-fed female LPP3^{OE} mice maintained a drastic reduction in plasma LPA concentration compared to HFD-fed LPP3^{FL} mice. In contrast, plasma LPA increased in HFD-fed male LPP3^{OE} mice and was similar compared to male HFD-fed LPP3^{FL} mice. LPA levels were similar between males and females within genotype and diet groups, except for increased LPA levels in male HFD-fed male LPP3^{OE} mice compared to female HFD-fed male LPP3^{OE} mice. Irrespective of diet and genotype, plasma LPA was lower in females compared to males.

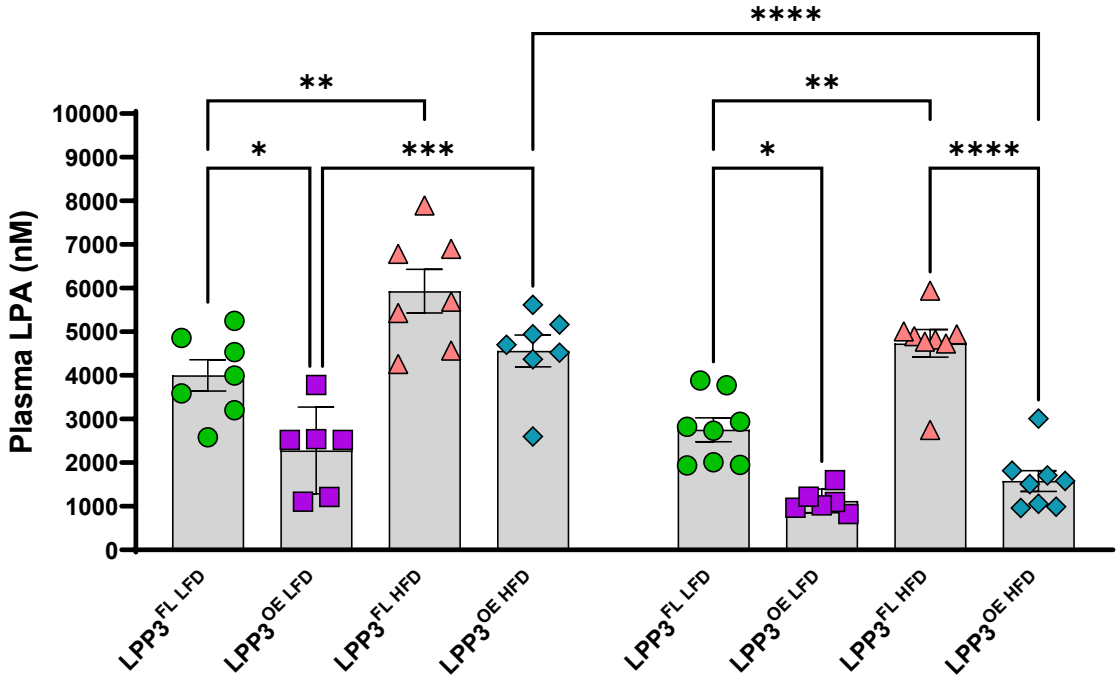

Figure 3.5. Cardiac specific LPP3 overexpression reduces plasma LPA levels in HFD-fed female but not male LPP3^{OE} mice. Plasma LPA levels were measured using a competitive ELISA kit in male and female 16-h fasted LFD -and HFD-fed LPP3^{FL} and LPP3^{OE} mice. Data are expressed as mean ± S.E.M. Statistical analysis were performed using two-way ANOVA followed by Tukey's multiple comparison test; n= 6-8; *p<0.05, **p< 0.01, ***P<0.001, ****p<0.0001

3.6 Female but not male LPP3^{OE} mice show reduced HFD-induced body weight gain and are protected from insulin resistance

Body weights of male and female mice were similar between control and LPP3 overexpressors prior to HFD feeding. HFD feeding significantly increased in body weight in male (Fig 3.6.2 A) and female LPP3^{FL} mice, respectively (Fig 3.6.1 A). Female HFD-fed LPP3^{OE} mice showed significantly reduced body weight compared to HFD-fed LPP3^{FL} mice (Fig 3.6.1 A,B). In agreement with lower body weight, female HFD-fed LPP3^{OE} showed reduced peripheral fat accumulation and PGAT weight compared to the HFD fed control mice (Fig 3.6.1 C,D). In contrast, male HFD-fed LPP3^{OE} mice showed similar body weight, peripheral fat accumulation, and PGAT weight compared to HFD-fed control mice (Fig 3.6.2 C, D). HFD feeding led to systemic glucose intolerance and insulin resistance as was assessed by GTT and ITT, respectively, in male and female control mice. While glucose intolerance was similar between female HFD-fed LPP3^{OE} and LPP3^{FL} mice, female LPP3^{OE} mice were completely protected from HFD-induced insulin resistance (Fig 3.6.1 E,F,G,H). Male HFD-fed LPP3^{OE} mice had augmented glucose intolerance and similar insulin resistance compared to LPP3^{FL} mice (Fig 3.6.2 E,F,G,H). Taken together, these data suggest that cardiac specific LPP3 overexpression protects female but not male mice from diet induced obesity and impaired systemic insulin sensitivity.

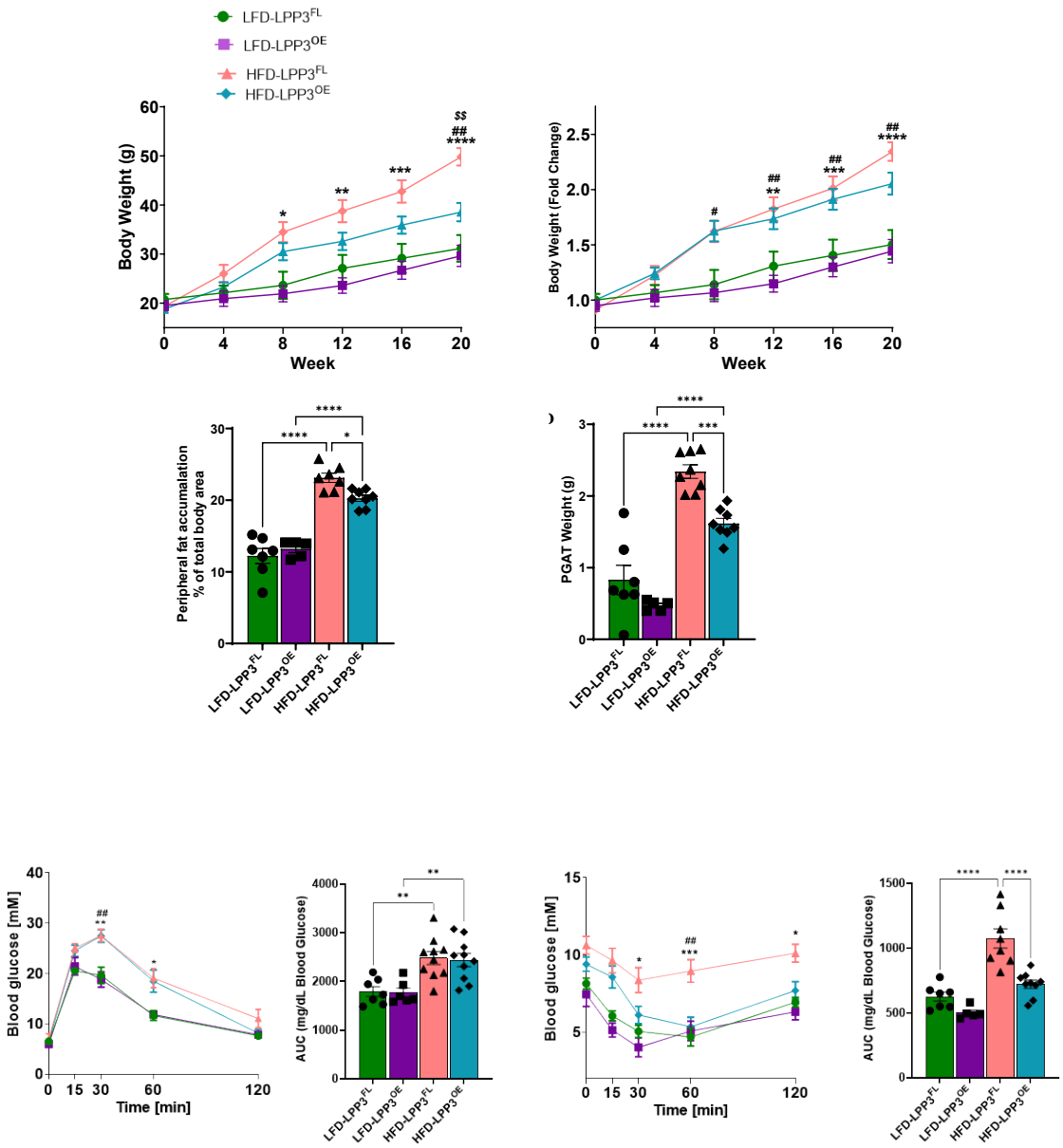
LFD-LPP3FL
LFD-LPP3OE
HFD-LPP3FL
HFD-LPP3OE
Body Weight (g)
Week
Body Weight (Fold Change)
Peripheral fat accumulation % of total body area
PGAT Weight (g)
Blood glucose [mM]
Time [min]
AUC (mg/dL Blood Glucose)

Figure 3.6.1. Female LPP3^{OE} mice are protected from diet-induced body weight gain and impaired insulin sensitivity. A) Absolute body weight; B) Body weight fold change; C) Peripheral fat accumulation; D) PGAT weight; E) GTT; F) AUC for GTT; G) ITT; H) AUC for ITT. Statistical analysis was performed by two-way ANOVA followed by Tukey's comparison's test (A,B,E,G) and one-way ANOVA (C,D,F,H); n = 6-10; ##p<0.01 for LFD-LPP3^{OE} vs. HFD-LPP3^{OE}, $$p<0.01 for HFD-LPP3^{FL} vs. HFD-LPP3^{OE} *p<0.05, **p<0.01, ***p<0.001 and ****p<0.0001 for LFD-LPP3^{FL} vs. HFD-LPP3^{FL}(A); *p<0.05, **p<0.01, ***p<0.001 and ****p<0.0001 for LFD-LPP3^{FL} vs. HFD-LPP3^{FL} , ##p<0.01 for LFD-LPP3^{OE} vs. HFD-LPP3^{OE}(B,E,G); *P<0.05 for HFD-LPP3^{FL} vs. HFD-LPP3^{OE}, ****p<0.0001 for LFD-LPP3^{FL} vs. HFD-LPP3^{FL} and LFD-LPP3^{OE} vs. HFD-LPP3^{OE}(C);***p<0.001 for HFD-LPP3^{FL} vs. HFD-LPP3^{OE}, ****p<0.0001 for LFD-LPP3^{FL} vs. HFD-LPP3^{FL} and LFD-LPP3^{OE} vs. HFD-LPP3^{OE}(D);**p<0.01 for LFD-LPP3^{FL} vs. HFD-LPP3^{FL};**p<0.01 for LFD-LPP3^{OE} vs. HFD-LPP3^{OE} (F); ****p<0.0001 for LFD-LPP3^{FL} vs HFD-LPP3^{FL} and HFD-LPP3^{OE} vs HFD-LPP3^{OE} (H).

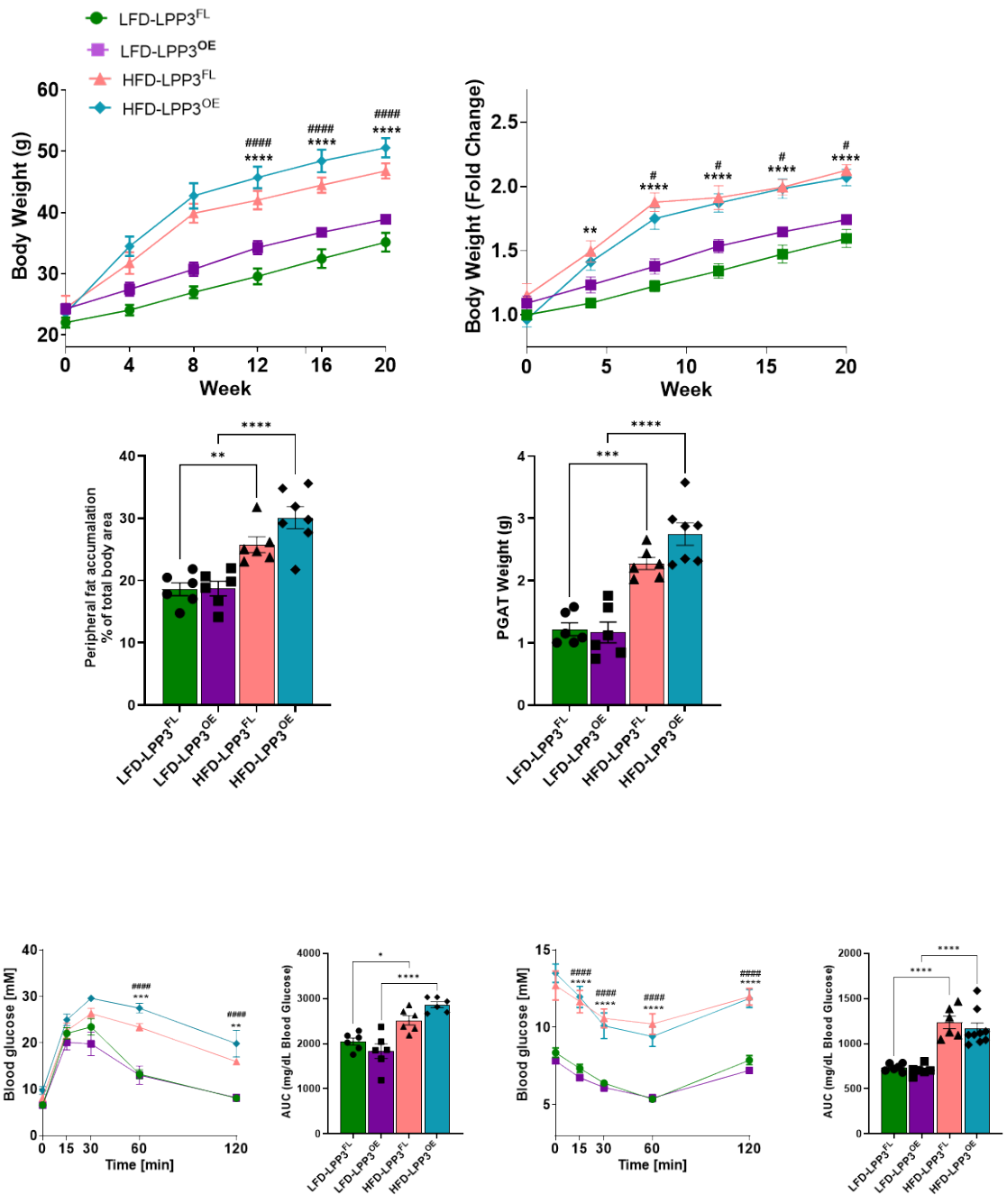
LFD-LPP3FL
LFD-LPP3OE
HFD-LPP3FL
HFD-LPP3OE
Body Weight (g)
Week
Body Weight (Fold Change)
Peripheral fat accumulation % of total body area
PGAT Weight (g)
Blood glucose [mM]
Time [min]
AUC (mg/dL Blood Glucose)

Figure 3.6.2. Male LPP3^{OE} mice are not protected from diet-induced body weight gain and impaired insulin sensitivity. A) Absolute body weight; B) Body weight fold change; C) Peripheral fat accumulation; D) PGAT weight; E) GTT; F) AUC for GTT; G) ITT; H) AUC for ITT. Statistical analysis was performed by two-way ANOVA followed by Tukey's comparison's test (A, B,E, F) and one-way ANOVA (C, D, F, H); n = 6-7; ####p<0.0001 for LFD-LPP3^{OE} vs. HFD-LPP3^{OE}, ****p<0.0001 for LFD-LPP3^{FL} vs. HFD-LPP3^{FL} (A); **p<0.01, ***p<0.001, ****p<0.0001 (B, C, E, G); **p<0.01 and ***p<0.001 for LFD-LPP3^{FL} vs. HFD-LPP3^{FL}, ####p<0.0001 for LFD-LPP3^{OE} vs. HFD-LPP3^{OE} (D); ****p<0.0001 for LFD-LPP3^{FL} vs. HFD-LPP3^{FL}, ####p<0.0001 for LFD-LPP3^{OE} vs. HFD-LPP3^{OE} (F).

3.7 Female but not male mice with cardiomyocyte-specific LPP3 overexpression are protected from HFD-induced cardiac dysfunction

A previous study using mice with cardiac-specific LPP3 deficiency has shown that LPP3 in cardiomyocytes is critical for cardiac function. Male cardiac-specific LPP3 knockout mice had significantly reduced left ventricular function which led to progressive heart failure[33]. Results from female mice were not reported in this study. Whether increasing LPP3 in cardiomyocytes influences cardiac function at baseline and following diet-induced obesity remains unclear. Therefore, we sought to determine the left ventricular function in LFD and HFD fed $LPP3^{OE}$ and $LPP3^{FL}$ mice using a pulsed-wave doppler system. Mitral inflow velocity signal represents the flow from the left atrium into the left ventricle during the diastolic phase of the cardiac cycle. Aortic outflow velocity signal is the result of myocardial contraction, leading to the systolic ejection of the blood within the left ventricle. We determined E/A ratio, IVCT and IVRT from mitral inflow pattern. Aortic peak velocity (APV) was analyzed from aortic outflow signal.

In female mice, heart rate was similar across groups except for a slight decrease in the LFD fed $LPP3^{OE}$ compared to $LPP3^{FL}$ mice (Figure. 3.7.1 A). HFD feeding resulted in a markedly increased E/A ratio in control mice, indicating diastolic dysfunction. E/A ratio was comparable between $LPP3^{OE}$ and $LPP3^{FL}$ mice on LFD. In contrast to $LPP3^{\mathbf{FL}}$ mice, E/A ratio was unaffected by HFD feeding in $LPP3^{OE}$ mice and was therefore considerably reduced in these mice when compared to HFD fed $LPP3^{FL}$ mice (Figure. 3.7.1 D). Similar to changes in E/A ratio, HFD feeding led to a prolongation of IVRT in $LPP3^{\mathbf{FL}}$ mice while HFD feeding did not cause changes to IVRT in $LPP3^{OE}$ mice (Figure. 3.7.1 E).

Collectively, the resistance of LPP3^{OE} mice towards HFD induced increases in E/A and IVRT suggest that these mice are protected from diastolic dysfunction. In addition to IVRT, IVCT was also prolonged in HFD fed LPP3^{FL} mice compared to LFD fed LPP3^{FL} mice while IVCT remained unchanged in LPP3^{OE} mice following HFD feeding (Figure. 3.7.1 E). In agreement with HFD-induced changes in IVCT, HFD fed LPP3$^{\mathbf{FL}}$ mice showed reduced APV compared to LFD-fed LPP3^{FL} mice, indicative of reduced cardiac output or systolic dysfunction in HFD-fed LPP3^{FL} mice. Strikingly, female LPP3^{OE} mice showed increased APV compared to LPP3^{FL} mice on both LFD and HFD. These data suggest that LPP3 overexpressing female mice have enhanced systolic function at baseline and under conditions of diet-induced obesity (Figure. 3.7.1 C). Interestingly, female LPP3^{OE} mice were also protected from a HFD induced increase in ventricle weight/tibia length ratio compared to LPP3^{FL} mice, suggesting that LPP3 overexpression protects female mice from HFD induced cardiac hypertrophy (Figure. 3.7.1 B).

In contrary to the females, HFD feeding led to an increase in heart rate in male mice in both genotypes and heart rate was elevated in male HFD-fed LPP3^{OE} compared to LPP3^{FL} mice (Figure. 3.7.2 A). Systolic and diastolic parameters were similar between LFD-fed male LPP3^{FL} and LPP3^{OE} mice. Both LPP3^{FL} and LPP3^{OE} mice showed increased E/A ratio and prolonged IVRT and IVCT on HFD (Figure. 3.7.2 D, E). Moreover, APV was significantly reduced in both HFD-fed male LPP3^{FL} and LPP3^{OE} mice compared to LFD-fed mice. Interestingly, HFD-fed male LPP3$^{\mathbf{OE}}$ mice showed significantly reduced APV compared to LPP3^{FL} mice (Figure. 3.7.2 C). These data suggest that, similar to male HFD-fed control mice, male LPP3 overexpressing mice have diastolic and systolic dysfunction after 19 weeks of HFD feeding. Male HFD-fed LPP3^{OE} mice also had an increased heart

weight/tibia length ratio compared to the LFD-fed mice, although heart weight/tibia length ratio was comparable between HFD-fed LPP3^{OE} and HFD-fed LPP3^{FL} mice (Figure. 3.7.2 B). In conclusion, cardiac specific LPP3 overexpression protected female but not male mice from HFD-induced diastolic and systolic dysfunction.

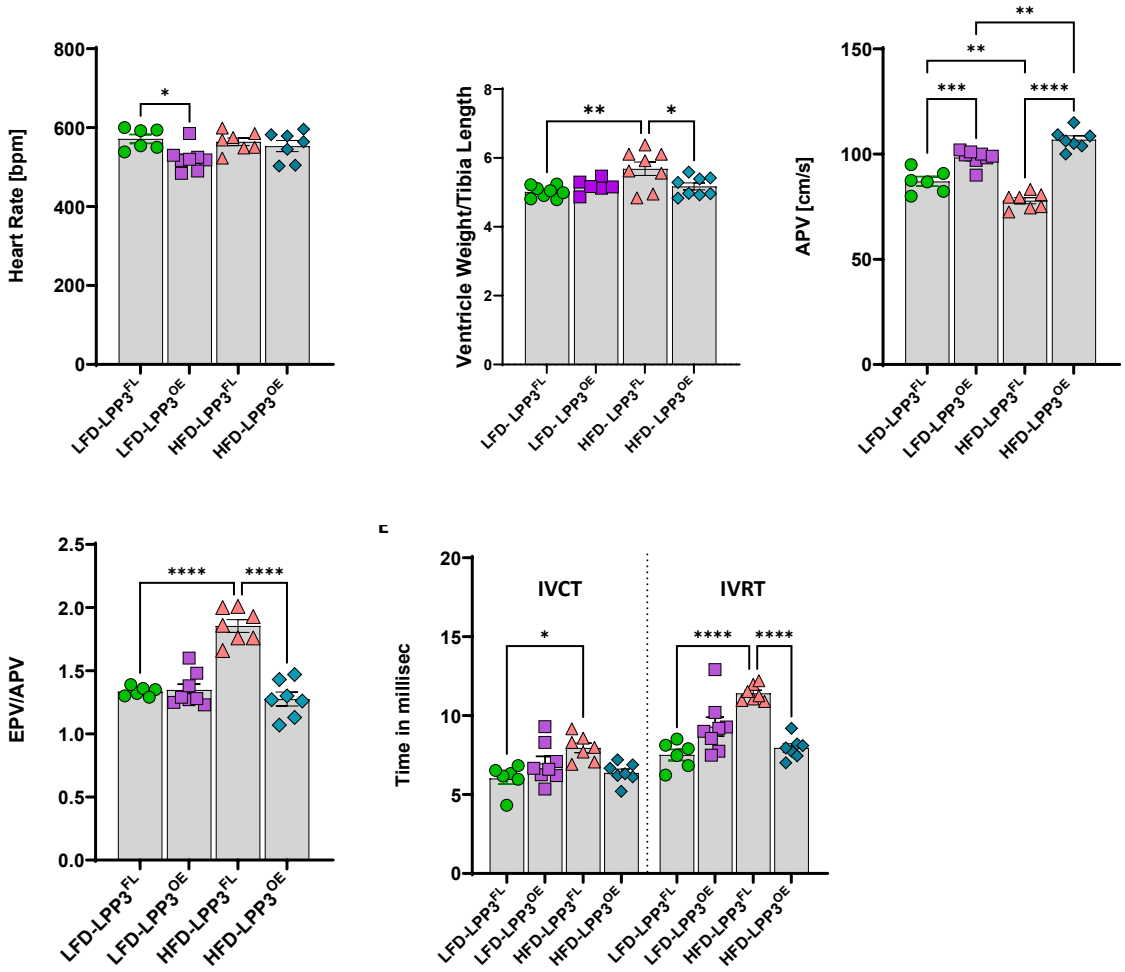

Figure 3.7.1 Female LPP3^{OE} mice are protected from HFD-induced cardiac dysfunction. A)Heart rate; B)Ventricle weight/Tibia length ratio; C) APV; D) E/A ratio; E) IVCT and IVRT. Data are expressed as mean ± S.E.M. Statistical analysis was performed using one-way ANOVA followed by Tukey's multiple comparison test; n=6-7; *p<0.05,**p<0.01, ***p<0.001, ****p<0.0001.

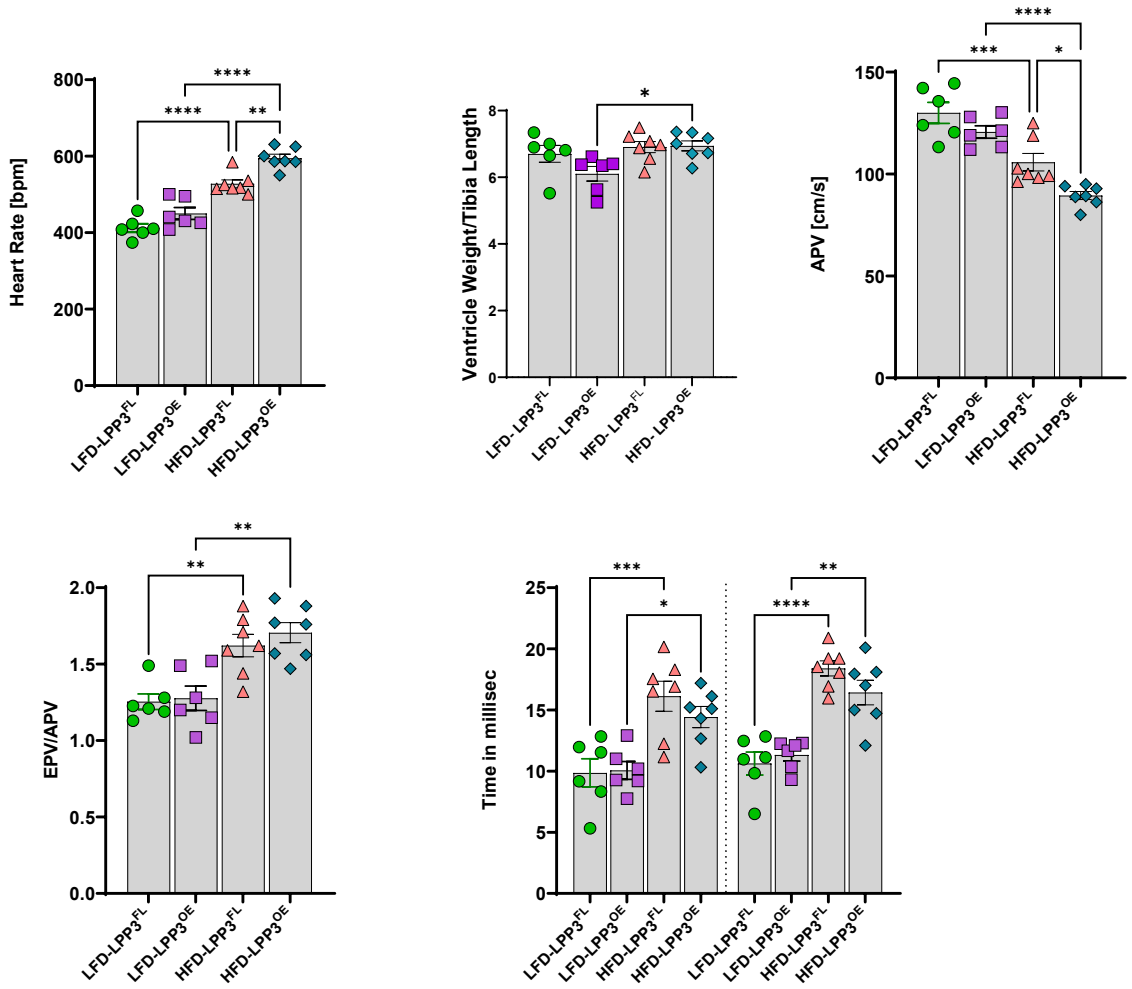

Figure 3.7.2: Male LPP3^{OE} mice are not protected from HFD-induced cardiac dysfunction. A) Heart rate; B) Ventricle weight/tibia length ratio; C) APV; D) E/A ratio; E) IVCT and IVRT. Data expressed as mean±S.E.M. Statistical analysis was performed using one way ANOVA followed by Tukey's multiple comparison test (B); n=6-7; *p<0.05,**p<0.01, ***p<0.001, ****p<0.0001.

3.8 Mitochondrial substrate metabolism in myofibers from HFD-fed LPP3^{OE} mice

We next wanted to determine whether mitochondrial respiration is altered by a high fat diet in LPP3^{OE} mice. Permeabilized myofibers from 16 h fasted male and female LFD- and HFD-fed LPP3^{FL} and LPP3^{OE} mice were examined for Pyr-linked respiration. In male and female LPP3^{FL} mice, Pyr-linked respiration was not significantly changed, but trended to be lower in HFD-fed mice compared to LFD fed mice (Figure. 3.8 A,C). Pyr-linked respiration in the presence of ADP was significantly increased in both LFD- and HFD-fed female LPP3^{OE} mice compared to LPP3^{FL} mice (Figure 3.8 A). In addition to this, complex II respiration upon rotenone addition and in the presence of succinate was also increased in LFD- and HFD-fed female LPP3^{OE} mice (Figure 3.8 A) as was uncoupled respiration (Figure 3.8 B). In males, we observed that after 20 weeks of high fat feeding, LPP3^{OE} mice had markedly reduced Pyr-linked and uncoupled respiration compared to the LFD-fed LPP3^{OE} mice, resulting in similar Pyr-linked and uncoupled respiration between male HFD-fed LPP3^{OE} and LPP3^{FL} mice (Figure 3.8 C, D). Taken together, these data suggest that cardiomyocyte specific LPP3 overexpression enhances Pyr-linked and uncoupled respiration in HFD-fed female but not male mice.

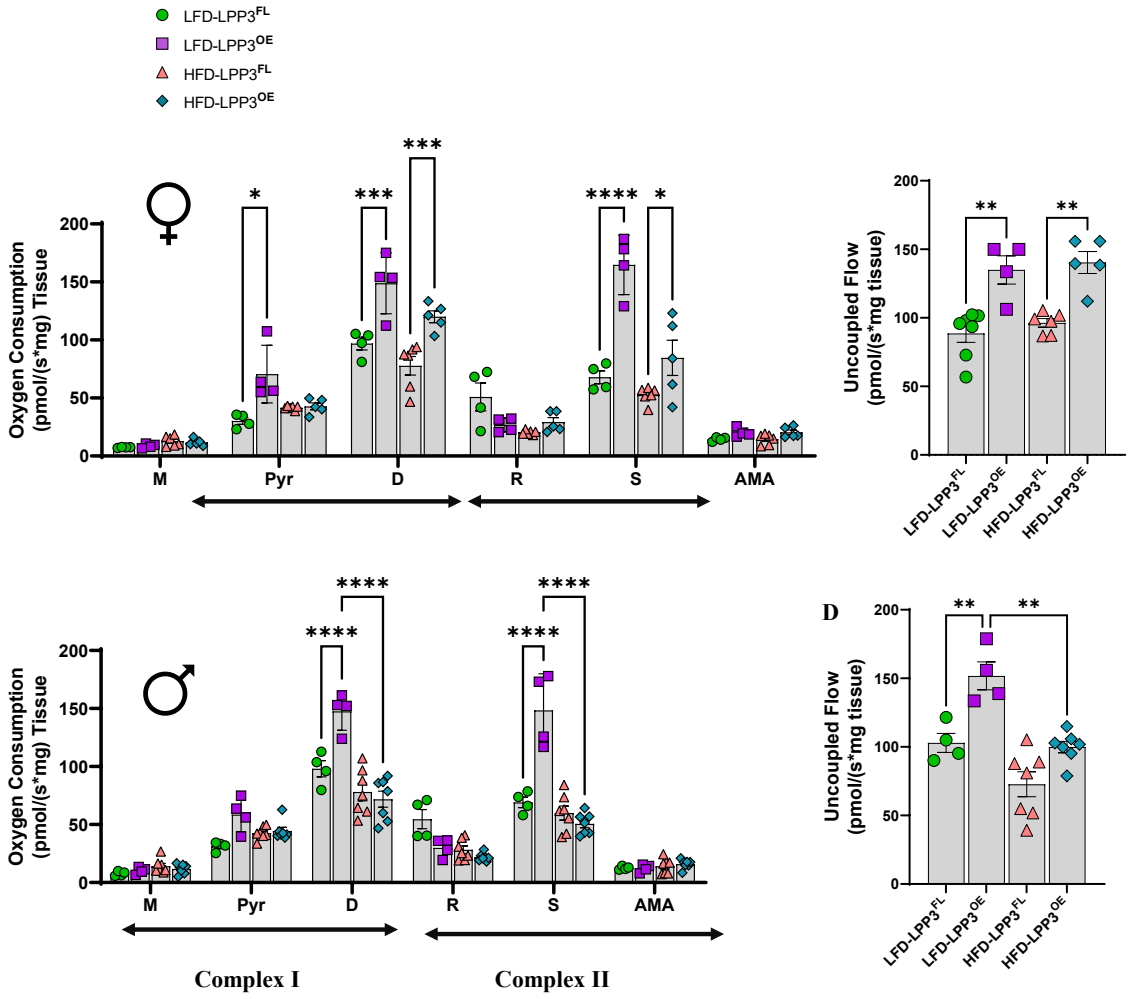

Figure 3.8. Pyr-linked and uncoupled respiration are enhanced in cardiac myofibers from HFD-fed female but not male LPP3^{OE} mice. A) Pyr-linked mitochondrial respiration in female mice; B) Uncoupled O_2 flow in female mice; C) Pyr-linked mitochondrial respiration in male mice; D) Uncoupled O_2 flow in male mice. Data are represented as mean± S.E.M. Statistical analysis was performed using two-way ANOVA followed by Tukey's multiple comparisons test; n = 4-7; *p<0.05,**p<0.01,***p<0.001,****p<0.0001. M-malate, Pyr- Pyruvate, D-Adenosine diphosphate, R- Rotenone, AMA- Antimycin A.

3.9 *Lpp3* mRNA levels in H9c2 cells incubated with high concentrations of fatty acids and in the heart from HFD-fed mice

To examine whether LPP3 levels are altered by a milieu containing high concentrations of fatty acids, we incubated differentiated H9c2 cells with either 1.2 mM palmitate, 1.2 mM oleate, or 1% BSA (control) for 16 h and determined *Lpp3* mRNA levels using quantitative PCR. High oleate treatment significantly increased *Lpp3* mRNA levels whereas high palmitate treatment did not alter *Lpp3* mRNA content (Figure. 3.9 A).

We next examined whether *Lpp3* mRNA levels in ventricular tissue are altered during diet induced obesity, a condition that is associated with elevated circulating fatty acids. Male C57BL/6J mice were fed HFD (60%) for 12 weeks, and body weight changes and *Lpp3* mRNA levels were determined. HFD-fed mice had significantly increased body weight after 12 weeks of HFD feeding compared to LFD mice (Figure. 3.9 B, data were obtained prior to my thesis work). Interestingly, *Lpp3* mRNA content was similar between groups (Figure. 3.9 C).

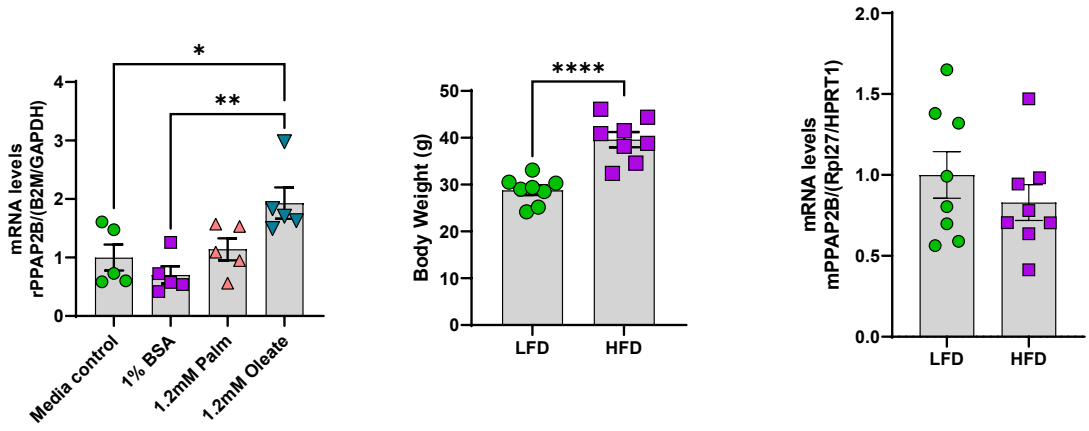

Figure 3.9. High oleate concentration increases *Lpp3* mRNA levels in H9c2 cells but cardiac *Lpp3* mRNA levels are unchanged in mice after 12 week HFD feeding. A) *Lpp*3 mRNA levels in H9c2 cells incubated with high palmitate or oleate. B) Body weight and C) *Lpp*3 mRNA levels in ventricular heart tissue from male mice fed high/low fat diet for 12 weeks. Data were normalized to B2M and GAPDH (A) and HPRT1 and RPL27 (C) reference genes. Graph represents mean± S.E.M.; Data are from three independent trails (A); Statistical analysis was performed using one way ANOVA followed by Tukey's multiple comparison test (A); n=5; and unpaired Student's t-test (B & C); n=5 (A); n=8 (B&C); *p<0.05, **p<0.01,****p<0.0001; A.U., arbitrary unit.

3.10 Validation of LPP3 knockdown using siRNA in H9c2 cells

To study the role of LPP3 in cellular functions in vitro, we aimed to silence *Lpp3* in H9c2 cardiomyoblasts using small interfering RNA (siRNA).

Differentiated H9c2 cells were transfected with a rat-specific anti-LPP3 siRNA at a concentration of 10 nM, and cells were harvested 48 h thereafter for analysis of *Lpp3* mRNA and protein levels. LPP3 siRNA decreased *Lpp3* mRNA levels by 60% compared to scrambled control siRNA as was determined by qPCR analysis (Fig 3.10 A). Correspondingly, LPP3 protein content was also reduced to a similar extent (Fig 3.10 B,C).

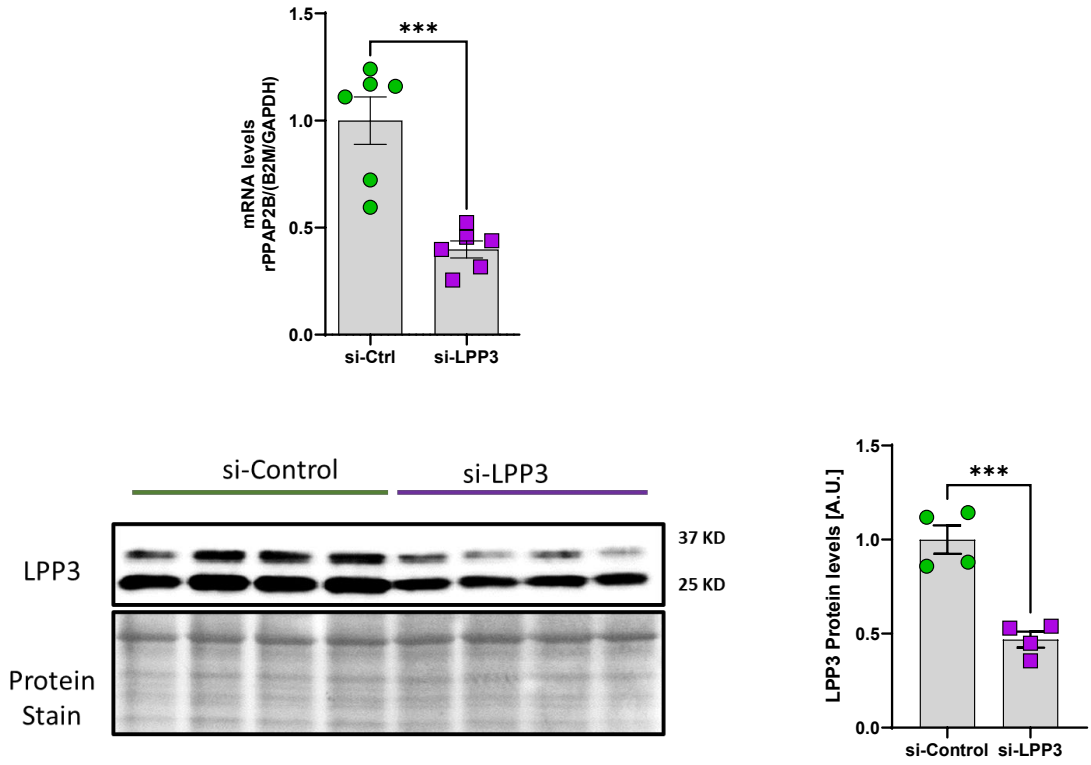

Figure 3.10. LPP3 knockdown using siRNA in H9c2 cells.
A) *Lpp3* mRNA levels in H9c2 cells transfected with anti-LPP3 or control siRNA. Data were normalized to B2M and GAPDH reference genes. B) Immunoblot and C) densitometric analysis of LPP3 protein levels. Data were normalized to protein stain. Graph represents mean±S.E.M.; Data are representative of two independent experiments; Statistical analysis was performed using unpaired Student's t-test (A & C), n = 4, A.U.; arbitrary unit. ***p<0.001.

3.11 LPP3 reduces cell survival in H9c2 cells

Cardiac-specific LPP3 deficiency leads to heart failure in mice, suggesting that LPP3 is necessary for cardiomyocyte function in vivo[39]. To assess whether a reduction in LPP3 influences viability of H9c2 cells in vitro, we knocked down LPP3 in H9c2 cells using siRNA for 48h, then estimated cell viability using the reduction of resazurin through the addition of PrestoBlue reagent in metabolically active cells. Incubation with doxorubicin (10 μM, DOX), a potent cytotoxic agent, served as positive control and a no-treatment group served as negative control. Knockdown of *Lpp3* reduced cell viability to 33% compared to the control group. Interestingly, the reduction in cell viability was similar in cells treated with LPP3 siRNA when compared to cells treated with a known cell death inducer, doxorubicin. This data indicates that even in the absence of serum, decline of *Lpp3* induced cell death in H9c2 cells, suggesting that *Lpp3* itself is essential for the cell survival. In conclusion, partial *Lpp3* knockdown in cardiomyocytes in vitro leads to a profound loss of cell viability and increased cell death. The mechanism behind the effect of LPP3 on cell survival is yet to be addressed.

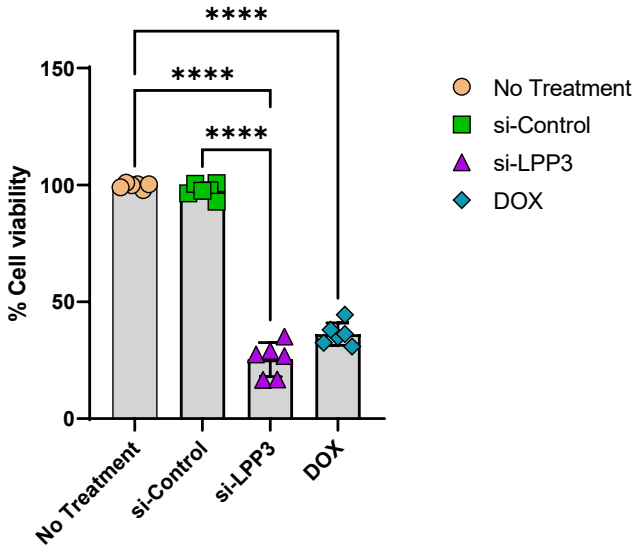

Figure 3.11. LPP3 knockdown reduces the viability of H9c2 cells.
Viability of H9c2 cells after siRNA mediated LPP3 knockdown for 48 hr. Data are represented as mean±S.E.M.; Data is representative of one experiment (and confirms observations made by other lab members); Statistical analysis was performed by one-way ANOVA followed by Tukey's post hoc test; n = 6; ***P<0.001, ****P<0.0001.

CHAPTER 4: DISCUSSION

Obesity-related cardiomyopathy is a leading cause of death worldwide. During obesity, circulating LPA levels are significantly elevated in murine obese models as well as in humans[40,41]. LPA is implicated as a major mediator of obesity-induced insulin resistance and impaired glucose homeostasis. Several studies have also shown that elevated levels of LPA induce cardiomyocyte hypertrophy[42,43]. Optimal LPA signaling depends on the balance between LPA production and degradation. Extracellular LPA is produced by ATX from LPC and is degraded through dephosphorylation by lipid LPPs to MAG. LPA signals through six distinct G-protein coupled receptors named LPA 1-6 and activates several pathways involved in cell migration, proliferation, and survival. The mammalian LPP family consists of three enzymes — LPP1 (PPAP2A), LPP2 (PPAP2C), and LPP3 (PPAP2B) — that are encoded by distinct genes (*PLPP1/PPAP2A*, *PLPP2/PPAP2C*, and *PLPP3/PPAP2B*, respectively)[24]. LPP3 is a key regulator of extracellular LPA levels and thereby LPA signaling, and LPP3 polymorphisms in humans and LPP3 deficiency in mice has been implicated in various pathophysiological conditions including CVDs[33,44] However, the role of LPP3 during obesity induced cardiac dysfunction remains unexplored. This study was the first to investigate the role of LPP3 expressed in cardiomyocytes in cardiac metabolism and function under obesogenic conditions.

A recent study using cardiomyocyte specific LPP3 knockout mice (CMLPP3-/-) showed reduced LPP activity in the heart and markedly increased plasma LPA levels compared to the control mice. This study suggests that LPP3 is the predominant LPP in the heart and plays an important role in the degradation of circulating LPA[33]. Also, culture of embryonic mouse fibroblasts lacking LPP3 resulted in a ~2.5-fold increase in extracellular (serum

derived) LPA. In this study intracellular LPA levels were undetectable[45]. CMLPP3-/- mice had enlarged hearts which was associated with progressive heart failure. Transmission electron micrograph analysis of the myocardium from eight-month-old CMLPP3−/− mice also showed extensive mitochondrial damage as was evidenced by cristae disorganization, vacuole formation, and rupture of the mitochondrial double membrane, which was associated with reduced mitochondrial respiration. This study suggests that cardiomyocyte LPP3 is critical for mitochondrial structure and function in the heart[33]. At present it is not known whether the detrimental effect of LPP3 deficiency on the heart is mediated by increased circulating LPA levels and/or involves other activities of LPP3, for example conversion of PA to DAG[46]. Consistent with this notion, when we silenced LPP3 in differentiated H9c2 cells resulting in a ~50% reduction in LPP3 protein (Fig 3.10), we observed an approximately 70% reduction in cell viability, demonstrating that even a relatively short-term decrease in LPP3 levels negatively influences H9c2 cell function. The active sites of LPP3 is not only present on the outer surface of cells but also on the luminal surface of ER and Golgi membranes[34]. However, PA is mainly produced by PLD which is on the cytosolic sides of the membranes, which is opposite to the catalytic domains of LPP3[47]. Interestingly, in HeLa cells LPP3 depletion decreased the levels of de novo synthesized DAG and the Golgi-associated DAG content and impaired protein trafficking in the early secretory pathway[34]. It is also possible that LPP3 exerts a similar role in cardiomyocytes which remains to be investigated. Together, these data suggest that LPP3 expressed in cardiomyocytes is indispensable for normal cardiac function. But the mechanism and significance of these observations needs to be explored further.

Increased LPA levels and LPA production through ATX are associated with several obesity related complications including T2D, cardiomyopathy, atherosclerosis, and hepatic steatosis. A recent study from our lab has shown that HFHS diet-fed whole body heterozygous ATX knockout mice have reduced ATX activity in serum and ameliorated insulin resistance compared to wild type mice, which was associated with improved insulin signaling in liver, PGAT, skeletal muscle, and heart in the ATX knockout mice. ATX knockout mice were also protected from HFHS diet-induced impairment of cardiomyocyte contractility as was assessed by sarcomere shortening analysis of isolated cardiomyocytes[18]. In agreement with this study, Weng et al. showed that inhibition of ATX using PF-8380 and the resulting lowering of circulating LPA levels attenuate HFD-induced cardiac hypertrophy, dysfunction and inflammation[41]. This study also showed that incubation with LPA increases cell size and stimulates inflammation in neonatal rat cardiomyocytes[41]. Moreover, circulating ATX levels were positively correlated with cardiac dysfunction and hypertrophy in humans[41]. Similarly, Xu et al. showed that ATX protein levels were increased in mice after HFD feeding[48]. Taken together, these studies point out that elevated LPA signaling in the myocardium is an important factor in obesity/HFD-related cardiac injury and that interrupting LPA signaling in cardiomyocytes may be a possible intervention to prevent and/or treat obesity cardiomyopathy. LPP3 inactivates LPA signaling by degrading extracellular LPA, among other extracellular and intracellular lipid phosphates such as PA, SIP and C1P[23,24]. Several studies have shown that systemic LPA levels increase with LPP3 reduction in liver, heart and adipose tissue in mice, suggesting that LPP3 modulation has the potential to alter extracellular LPA levels and thus cellular LPA signaling[45,49].

Thus, the overall goal of my thesis was to determine whether increased expression of LPP3 in cardiomyocytes can protect from obesity cardiomyopathy. We used the Cre/LoxP system to overexpress LPP3 specifically in cardiomyocytes from C57BL/6J mice. I examined circulating LPA levels, systemic glucose homoeostasis, body & ventricle weight, cardiomyocyte mitochondrial respiration, and cardiac function in these animals to understand whether and how LPP3 overexpression influences the adult myocardium under healthy and obese conditions.

To date, few studies have addressed whether LPP3 levels are altered in the myocardium during obesity. A recent study showed that LPP3 protein levels are increased in the heart from HFD-fed male mice via a mechanism that involves the microRNA (miRNA), miR-184[46]. Mao *et al.* showed that LPP3 upregulation during inflammation involves the NF-κb transcription factor complex in HEK293T cells[50]. It is not known whether the NF-κb regulates LPP3 expression also in cardiomyocytes. On the contrary, in our lab, we found that LPP3 protein levels are reduced in atrial appendages from obese compared to non-obese humans (unpublished data). We also show that *Lpp3* mRNA was unchanged in mice fed HFD for 12 weeks, although it remains to be determined if HFD feeding for longer durations influences *Lpp3*mRNA and protein levels in the heart and cardiomyocyte.

LPP3 overexpression in cardiomyocytes reduced circulating LPA levels in both male and female mice at baseline, demonstrating that increased LPP3 expression in cardiomyocytes is sufficient to lower systemic LPA levels (Figure 3.1 F,H). Interestingly, LPA levels in LFD- and HFD-fed control mice were comparable between males and females (Fig 3.5). To our understanding, this is the first report of LPA plasma level comparison between male and female mice. Interestingly, in humans, it was reported that females have significantly

higher circulating LPA levels compared to males[22], indicating fundamental differences in the sex-dependent regulation of LPA levels and metabolism between mice and humans that warrant further investigation. In agreement with prior studies examining LPA levels in obese mice, we show an increase in plasma LPA levels following HFD feeding in male and female control mice (Fig 3.5). While a reduction in plasma LPA levels was maintained in HFD-fed female LPP3^{OE} mice compared to the LPP3^{FL} mice, LPP3 overexpression failed to reduce plasma LPA in male HFD-fed mice. It is possible that increased LPA production by ATX compensates for increased LPP3 expression in HFD-fed male mice.

Elevated LPA levels during obesity are associated with several complications including impaired insulin sensitivity and mitochondrial dysfunction. Several studies have shown that increased LPA levels reduce tissue insulin signaling both *in vivo* and *in vitro*. For example, our lab showed that increased ATX levels (and thus LPA production) contribute to impaired insulin stimulated AKT and p70S6K phosphorylation in the heart in HFHS-fed mice compared with chow-fed mice. Moreover, C2C12 cells had reduced insulin-stimulated AKT phosphorylation following incubation with LPA[18]. In these cells, incubation with LPA also exacerbated palmitate-induced impairment of insulin signaling[18]. Similarly, incubation of primary rat hepatocytes with LPA inhibited insulin-stimulated AKT phosphorylation and glycogen synthesis via LPA3 receptor[51]. As we observed a reduction in circulating LPA levels in our LPP3 overexpressing model, we determined insulin signaling in these mice *in vivo* by assessing AKT phosphorylation. Insulin stimulated AKT phosphorylation at S473 and T308 was comparable between chow diet-fed control and LPP3 overexpressing mice (Fig 3.3 A,B,C). Notably, cardiac insulin signaling was also similar between chow-fed ATX KO Het and WT mice[18]. Differences in

cardiac insulin signaling precipitated only after high fat feeding in these mice. Therefore, it remains to be determined whether cardiac insulin signaling is altered by LPP3 overexpression in HFD-fed mice. It is possible that LPP3 overexpression enhances insulin signaling only under conditions that promote cardiac insulin resistance.

LPA signaling has also been shown to influence substrate linked mitochondrial respiration. Isolated mitochondria from the myocardium and neonatal cardiomyocytes from CMLPP3-/- mice showed a reduction in basal oxygen consumption rate in presence of glucose as substrate, mitochondrial ATP production and maximal respiration when compared to mitochondria from the control mice. These data were recapitulated in neonatal cardiomyocytes from CMLPP3-/- mice, where also a compensatory increase in glycolysis was observed. Neonatal cardiomyocytes from CMLPP3-/- mice also showed higher superoxide levels when treated with LPA as compared to cardiomyocytes from the LPA treated control mice. When LPP3 was reintroduced, superoxide levels were reduced in CMLPP3-/- cardiomyocytes[33]. These findings suggest that LPP3 is critical for respiration and function of myocardial mitochondria, although it is unclear whether mitochondrial function defects were a direct result of LPP3 deficiency or secondary to heart failure development. In addition, our lab showed that LPA incubation of C2C12 cells impairs mitochondrial respiration in the presence of fatty acylcarnitine and pyruvate, suggesting that LPA signaling hinders mitochondrial respiration in both cardiac and skeletal muscle cells[18]. We show that LPP3 overexpression specifically in cardiomyocytes enhances pyruvate/glucose but not fatty acylcarnitine-linked respiration in isolated cardiac myofibers from both male and female chow/LFD-fed mice. Our data also show that increased pyruvate/glucose linked respiration is preserved in female but not male mice with

LPP3 overexpression following HFD feeding, which was associated with a reduction in plasma LPA levels in HFD-fed female LPP3^{OE} mice but not in male LPP3^{OE} mice (Fig 3.8).

Several studies have demonstrated that increased LPA levels/LPA production through ATX during obesity impairs systemic glucose homeostasis, insulin sensitivity, and cardiac function. However, only few studies have explored the role of LPP3 in obesity-induced metabolic complications. Interestingly, male and female Western diet fed adipose specific LPP3 knockout mice had improved glucose tolerance and reduced plasma insulin levels compared to control despite unchanged systemic LPA levels and adiposity. Western diet fed adipose LPP3 knockout mice had blunted ceramide and sphingomyelin accumulation in adipose tissue, increased levels of sphingosine 1-phosphate, and reduced expression of serine palmitoyl transferase, identifying an unexpected role for LPP3 in diet-dependent sphingolipid synthesis[49].

In our study, HFD fed female LPP3 overexpressing mice were protected from excess body weight gain and adipose tissue accumulation, and exhibited improved insulin sensitivity, which was associated with reduced plasma LPA levels (Fig 3.6.1 A,B,C,D,G,H). However, glucose tolerance was similar between the genotypes (Fig 3.6.1 E,F). It is possible that female HFD-fed LPP3^{OE} mice maintain similar glucose tolerance compared to control at lower plasma insulin levels, which should be determined in future. In contrast to female LPP3^{OE} mice, male LPP3^{OE} mice gained body weight and accumulated adipose tissue similarly compared to control mice on a HFD (Fig 3.6.2 A,B,C,D). Male HFD-fed LPP3^{OE} mice also showed slightly exacerbated glucose intolerance and similarly impaired insulin sensitivity when compared to the HFD-fed control mice (Fig 3.6.2 E,F,G,H). The

mechanisms underlying the sex differences observed in HFD-induced obesity and systemic metabolic perturbations in LPP3^{OE} mice warrant further examination. It is possible that increases in circulating LPA levels in HFD-fed male but not female LPP3 OE mice contribute to these metabolic changes in male mice.

My thesis work culminated in the analysis of *in vivo* cardiac function in LFD- and HFD-fed LPP3^{OE} mice to determine whether cardiac-specific LPP3 overexpression alters cardiac function at baseline and under obesogenic conditions. On LFD, male and female LPP3^{OE} mice had similar systolic and diastolic cardiac function, demonstrating that cardiac-specific LPP3 overexpression does not alter cardiac function at baseline. While HFD feeding caused a cardiac function decline in male and female control mice, both systolic and diastolic function were preserved in female LPP3^{OE} mice which was not observed in male LPP3^{OE} mice. Female LPP3 overexpressing mice maintained similar E/A ratio and IVRT, indicators of diastolic function, and APV and IVCT, indicators of systolic function, with no change in heart rate when compared to LFD-fed mice (Fig 3.7.1 A,B,C,D,E). Female LPP3^{OE} mice were also protected from HFD-induced cardiac hypertrophy. In males, we observed an opposite trend with impaired diastolic and systolic dysfunction in HFD-fed compared to LFD fed LPP3^{OE} mice. Strikingly, the heart rate was increased in both genotypes with HFD feeding in males (Fig 3.7.2). This data is consistent with a prior study that also showed an elevated heart rate in male mice with diet-induced obesity[52].

One of the major mechanisms that link LPA signaling to insulin sensitivity is mitochondrial function. LPP3 overexpression ameliorated Pyr-linked respiration in HFD-fed female LPP3^{OE} mice but not in male LPP3^{OE} mice. In fact, HFD-fed male LPP3^{OE} mice showed significantly reduced mitochondrial respiration compared to the LFD-fed male LPP3^{OE}

mice (Fig 3.8 C,D). Succinate linked complex II respiration was increased in both male and female LPP3$^{\mathbf{OE}}$ mice at baseline whereas this was only maintained in females after high fat feeding (Fig 3.8 A,B). Uncoupled respiration was also enhanced in both male and female LPP3^{OE} mice at baseline and remained increased only in female LPP3^{OE} mice following HFD feeding.

CHAPTER 5: CONCLUSIONS AND FUTURE DIRECTIONS

This study was the first to investigate the influence of cardiomyocyte specific LPP3 overexpression on cardiac mitochondrial metabolism and function under healthy and obesogenic conditions. This study yielded three major insights: 1) Cardiomyocyte specific LPP3 overexpression was sufficient to reduce plasma LPA levels in both males and females at baseline and exclusively in females following HFD feeding; 2) Cardiomyocyte specific LPP3 overexpression increased Pyr-linked respiration in both males and females at baseline and exclusively in females following HFD feeding; 3) Female but not male LPP3 overexpressing mice are protected from HFD-induced excess body weight gain, adipose tissue accumulation, insulin resistance, and cardiac dysfunction. In conclusion, cardiac specific LPP3 overexpression has a protective effect against HFD-induced cardiometabolic dysfunction in female but not male mice. Therefore, targeted LPP3 activation could possibly be developed as a preventative or therapeutic intervention for obesity cardiomyopathy, particularly in females.

The mechanism by which LPP3 overexpression protects female but not male mice needs further investigation. It is possible that differences in LPA receptor levels between male and female cardiomyocytes contribute to these observed sex differences in mitochondrial metabolism and cardiac function. Thus, protein levels of LPA1-6 receptors should be determined in cardiomyocytes from LFD- and HFD-fed male and female mice. In addition to this, ATX levels needs to be assessed as previous studies have shown the role of ATX in regulating circulating LPA levels. Also, the subcellular localization of LPP3 in cardiomyocytes during obesity and healthy conditions must be evaluated. Comprehensive lipidomic analysis needs to be done to understand whether LPP3 overexpression changes

lipids other than LPA in cardiomyocytes. To understand the mechanism behind the enhanced Pyr-linked respiration in LPP3 overexpressing mice, proteins and enzymes regulating mitochondrial respiration need to be assessed, for example mitochondrial pyruvate carrier. Also, it will also be important to clarify if sex hormones play any role in the phenotypic and metabolic differences observed between male and female LPP3 overexpressing mice. Due to high toxicity of LPP3 knockdown in H9c2 cells, we couldn't further examine its effect on mitochondrial metabolism and function. Alternate cell models, for example the human AC16 cells, could be explored for studies involving LPP3 knockdown. Future studies will need to define specific signaling pathways that link the LPA-LPP3 axis to heart function and mitochondrial metabolism. These studies will also allow us to better assess whether targeting the LPA-LPP3 signaling axis could hold promise as a treatment for obesity-induced cardiac dysfunction.

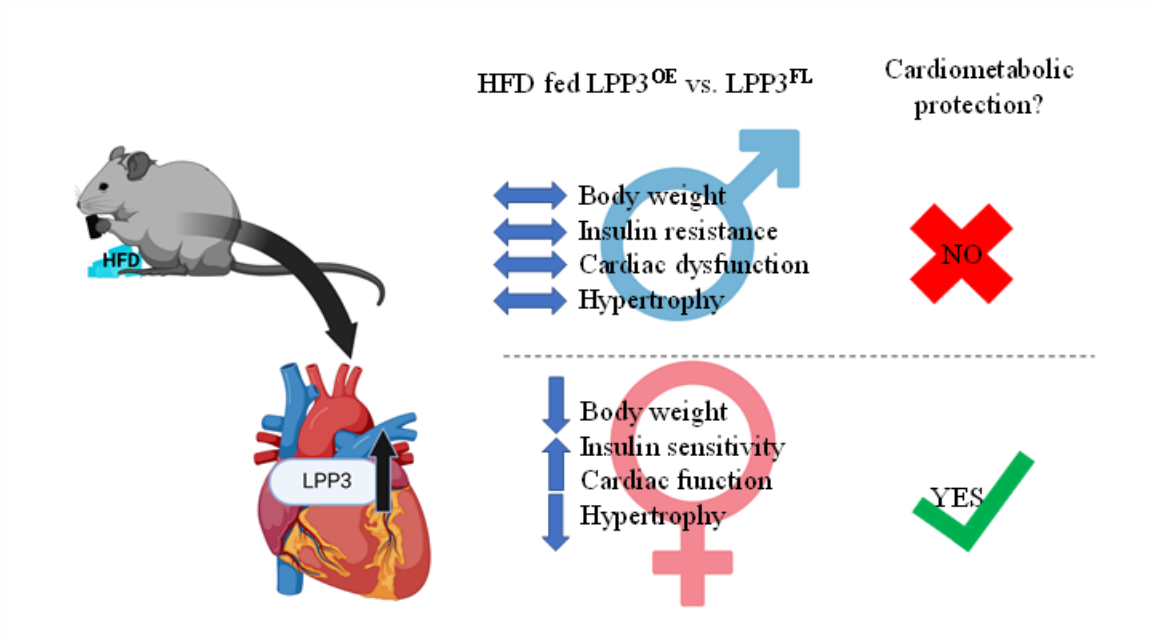

Figure 4: Summary of key observations from HFD-fed LPP3^{OE} mice.

REFERENCES

1. Mittendorfer, B. Origins of metabolic complications in obesity: Adipose tissue and free fatty acid trafficking. *Curr. Opin. Clin. Nutr. Metab. Care* **14**, 535–541 (2011).

2. American Heart Association. 2021 Heart Disease & Stroke Statistical Update Fact Sheet Global Burden of Disease High Blood Cholesterol and Other Lipids. *Am. Hear. Assoc.* 2019–2021 (2021).

3. Cercato, C. & Fonseca, F. A. Cardiovascular risk and obesity. *Diabetol. Metab. Syndr.* **11**, 1–15 (2019).

4. Chait, A. & den Hartigh, L. J. Adipose Tissue Distribution, Inflammation and Its Metabolic Consequences, Including Diabetes and Cardiovascular Disease. *Front. Cardiovasc. Med.* **7**, 1–41 (2020).

5. Jung, U. J. & Choi, M. S. Obesity and its metabolic complications: The role of adipokines and the relationship between obesity, inflammation, insulin resistance, dyslipidemia and nonalcoholic fatty liver disease. *Int. J. Mol. Sci.* **15**, 6184–6223 (2014).

6. Lipke, K., Kubis-Kubiak, A. & Piwowar, A. Molecular Mechanism of Lipotoxicity as an Interesting Aspect in the Development of Pathological States—Current View of Knowledge. *Cells* **11**, (2022).

7. Consitt, L. A., Bell, J. A. & Houmard, J. A. Intramuscular lipid metabolism, insulin action, and obesity. *IUBMB Life* **61**, 47–55 (2009).

8. Alves-Bezerra, M. & Cohen, D. E. Triglyceride metabolism in the liver. *Compr. Physiol.* **8**, 1–22 (2018).

9. Klop, B., Elte, J. W. F. & Cabezas, M. C. Dyslipidemia in Obesity: Mechanisms and Potential Targets. *Nutrients* **5**, 1218–1240 (2013).

10. Ren, J., Wu, N. N., Wang, S., Sowers, J. R. & Zhang, Y. Obesity cardiomyopathy: Evidence, mechanisms, and therapeutic implications. *Physiol. Rev.* **101**, 1745–1807 (2021).

11. Neubauer, S. The Failing Heart — An Engine Out of Fuel. *N. Engl. J. Med.* **356**, 1140–1151 (2007).

12. Stanley, W. C., Recchia, F. A. & Lopaschuk, G. D. Myocardial substrate metabolism in the normal and failing heart. *Physiol. Rev.* **85**, 1093–1129 (2005).

13. Randle, P. J., Garland, P. B., Hales, C. N. & Newsholme, E. A. the Glucose Fatty-Acid Cycle Its Role in Insulin Sensitivity and the Metabolic Disturbances of Diabetes Mellitus. *Lancet* **281**, 785–789 (1963).

14. Alrob, O. A. *et al.* Obesity-induced lysine acetylation increases cardiac fatty acid oxidation and impairs insulin signalling. *Cardiovasc. Res.* **103**, 485–497 (2014).

15. Peterson, L. R. *et al.* Effect of Obesity and Insulin Resistance on Myocardial Substrate Metabolism and Efficiency in Young Women. *Circulation* **109**, 2191–2196 (2004).

16. Makrecka-Kuka, M. *et al.* Altered mitochondrial metabolism in the insulin-resistant heart. *Acta Physiol.* **228**, 1–26 (2020).

17. Perrakis, A. & Moolenaar, W. H. Thematic Review Series: Lysophospholipids and their Receptors: Autotaxin: Structure-function and signaling. *J. Lipid Res.* **55**, 1010–1018 (2014).

18. D'Souza, K. *et al.* Autotaxin-LPA signaling contributes to obesity-induced insulin resistance in muscle and impairs mitochondrial metabolism. *J. Lipid Res.* **59**, 1805–1817 (2018).

19. Sheng, X., Yung, Y. C., Chen, A. & Chun, J. Lysophosphatidic acid signalling in development. *Dev.* **142**, 1390–1395 (2015).

20. MacAulay, K. & Woodgett, J. R. Targeting glycogen synthase kinase-3 (GSK-3) in the treatment of Type 2 diabetes. *Expert Opin. Ther. Targets* **12**, 1265–1274 (2008).

21. Yap, J. *et al.* Association of diabetes mellitus on cardiac remodeling, quality of life, and clinical outcomes in heart failure with reduced and preserved ejection fraction. *J. Am. Heart Assoc.* **8**, (2019).

22. Michalczyk, A., Budkowska, M., Dołęgowska, B., Chlubek, D. & Safranow, K. Lysophosphatidic acid plasma concentrations in healthy subjects: Circadian rhythm and associations with demographic, anthropometric and biochemical parameters. *Lipids Health Dis.* **16**, 1–9 (2017).

23. Jose, A. & Kienesberger, P. C. Autotaxin-LPA-LPP3 axis in energy metabolism and metabolic disease. *Int. J. Mol. Sci.* **22**, (2021).

24. Tang, X., Benesch, M. G. K. & Brindley, D. N. Lipid phosphate phosphatases and their roles in mammalian physiology and pathology. *J. Lipid Res.* **56**, 2048–2060 (2015).

25. D'Souza, K. *et al.* Autotaxin is regulated by glucose and insulin in adipocytes. *Endocrinology* **158**, 791–803 (2017).

26. Chen, J. *et al.* Specific LPA receptor subtype mediation of LPA-induced hypertrophy of cardiac myocytes and involvement of Akt and NFκB signal pathways. *J. Cell. Biochem.* **103**, 1718–1731 (2008).

27. Pei, J. *et al.* LPA2Contributes to Vascular Endothelium Homeostasis and Cardiac Remodeling After Myocardial Infarction. *Circ. Res.* **131**, 388–403 (2022).

28. Kraemer, M. P. *et al.* Effects of diet and hyperlipidemia on levels and distribution of circulating lysophosphatidic acid. *J. Lipid Res.* **60**, 1818–1828 (2019).

29. Brown, A. *et al.* Lysophosphatidic acid receptor mRNA levels in heart and white adipose tissue are associated with obesity in mice and humans. *PLoS One* **12**, 1–23 (2017).

30. Tomsig, J. L. *et al.* Lipid phosphate phosphohydrolase type 1 (LPP1) degrades extracellular lysophosphatidic acid in vivo. *Biochem. J.* **419**, 611–618 (2009).

31. Yue, J. *et al.* Mice with transgenic overexpression of lipid phosphate phosphatase-1 display multiple organotypic deficits without alteration in circulating lysophosphatidate level. *Cell. Signal.* **16**, 385–399 (2004).

32. Zhang, N., Sundberg, J. P. & Gridley, T. Mice mutant for Ppap2c, a homolog of the germ cell migration regulator wunen, are viable and fertile. *Genes. (United States)* **27**, 137–140 (2000).

33. Chandra, M. *et al.* Cardiac-specific inactivation of LPP3 in mice leads to myocardial dysfunction and heart failure. *Redox Biol.* **14**, 261–271 (2018).

34. Gutierrez-Martínez, E. *et al.* Lipid phosphate phosphatase 3 participates in transport carrier formation and protein trafficking in the early secretory pathway. *J. Cell Sci.* **126**, 2641–2655 (2013).

35. Busnelli, M. *et al.* Liver-specific deletion of the Plpp3 gene alters plasma lipid composition and worsens atherosclerosis in apoE -/- mice. *Sci. Rep.* **7**, 1–13 (2017).

36. Van Hoose, P. M. *et al.* Lipid phosphate phosphatase 3 in smooth muscle cells regulates angiotensin II-induced abdominal aortic aneurysm formation. *Sci. Rep.* **12**, 1–12 (2022).

37. Kano, K. *et al.* Suppressing postcollection lysophosphatidic acid metabolism improves the precision of plasma LPA quantification. *J. Lipid Res.* **62**, 100029 (2021).

38. Perez, L. J. *et al.* Validation of optimal reference genes for quantitative real time PCR in muscle and adipose tissue for obesity and diabetes research. *Sci. Rep.* **7**, 1–13 (2017).

39. Chandra, M. *et al.* Cardiac-specific inactivation of LPP3 in mice leads to myocardial dysfunction and heart failure. *Redox Biol.* **14**, 261–271 (2018).

40. D'Souza, K., Paramel, G. V. & Kienesberger, P. C. Lysophosphatidic acid signaling in obesity and insulin resistance. *Nutrients* **10**, 10–15 (2018).

41. Weng, J. *et al.* Autotaxin/lysophosphatidic acid signaling mediates obesity-related cardiomyopathy in mice and human subjects. *J. Cell. Mol. Med.* **23**, 1050–1058 (2019).

42. Yang, J. *et al.* Lysophosphatidic acid is associated with cardiac dysfunction and hypertrophy by suppressing autophagy via the LPA3/AKT/mTOR pathway. *Front. Physiol.* **9**, 1–14 (2018).

43. Raja, A. A. *et al.* Ablation of lysophosphatidic acid receptor 1 attenuates hypertrophic cardiomyopathy in a mouse model. *Proc. Natl. Acad. Sci. U. S. A.* **119**, 1–12 (2022).

44. Chabowski, D. S. *et al.* Lipid phosphate phosphatase 3 maintains NO-mediated flow-mediated dilatation in human adipose resistance arterioles. *J. Physiol.* **601**, 469–481 (2023).

45. Escalante-Alcalde, D. *et al.* The lipid phosphatase LPP3 regulates extra-embryonic vasculogenesis and axis patterning. *Development* **130**, 4623–4637 (2003).

46. Chang, W., Fa, H., Xiao, D. & Wang, J. MicroRNA-184 alleviates insulin resistance in cardiac myocytes and high fat diet-induced cardiac dysfunction in mice through the LPP3/DAG pathway. *Mol. Cell. Endocrinol.* **508**, 110793 (2020).

47. Bruntz, R. C., Lindsley, C. W. & Brown, H. A. Phospholipase D signaling pathways and phosphatidic acid as therapeutic targets in cancer. *Pharmacol. Rev.* **66**, 1033–1079 (2014).

48. Xu, Y. *et al.* Adipose tissue-derived autotaxin causes cardiomyopathy in obese mice. *J. Mol. Endocrinol.* **63**, 113–121 (2019).

49. Federico, L. *et al.* Lipid phosphate phosphatase 3 regulates adipocyte sphingolipid synthesis, but not developmental adipogenesis or diet-induced obesity in mice. *PLoS One* **13**, 1–14 (2018).

50. Mao, G., Smyth, S. S. & Morris, A. J. Regulation of PLPP3 gene expression by NF-κB family transcription factors. *J. Biol. Chem.* **294**, 14009–14019 (2019).

51. Fayyaz, S. *et al.* Lysophosphatidic Acid Inhibits Insulin Signaling in Primary Rat Hepatocytes via the LPA 3 Receptor Subtype and is Increased in Obesity. *Cell. Physiol. Biochem.* **43**, 445–456 (2017).

52. Bruder-Nascimento, T., Ekeledo, O. J., Anderson, R., Le, H. B. & Belin de Chantemèle, E. J. Long term high fat diet treatment: An appropriate approach to study the sex-specificity of the autonomic and cardiovascular responses to obesity in mice. *Front. Physiol.* **8**, 1–11 (2017).